Sources of Intermodel Spread in the Lapse Rate and Water Vapor Feedbacks

STEPHEN PO-CHEDLEY

Lawrence Livermore National Laboratory, Livermore, California

KYLE C. ARMOUR

Department of Atmospheric Sciences, and School of Oceanography, University of Washington, Seattle, Washington

CECILIA M. BITZ

Department of Atmospheric Sciences, University of Washington, Seattle, Washington

MARK D. ZELINKA AND BENJAMIN D. SANTER

Lawrence Livermore National Laboratory, Livermore, California

QIANG FU

Department of Atmospheric Sciences, University of Washington, Seattle, Washington

(Manuscript received 11 October 2017, in final form 29 December 2017)

ABSTRACT

Sources of intermodel differences in the global lapse rate (LR) and water vapor (WV) feedbacks are assessed using CO_2 forcing simulations from 28 general circulation models. Tropical surface warming leads to significant warming and moistening in the tropical and extratropical upper troposphere, signifying a nonlocal, tropical influence on extratropical radiation and feedbacks. Model spread in the locally defined LR and WV feedbacks is pronounced in the Southern Ocean because of large-scale ocean upwelling, which reduces surface warming and decouples the surface from the tropospheric response. The magnitude of local extratropical feedbacks across models and over time is well characterized using the ratio of tropical to extratropical surface warming. It is shown that model differences in locally defined LR and WV feedbacks, particularly over the southern extratropics, drive model variability in the global feedbacks. The cross-model correlation between the global LR and WV feedbacks therefore does not arise from their covariation in the tropics, but rather from the pattern of warming exerting a common control on extratropical feedback responses. Because local feedbacks over the Southern Hemisphere are an important contributor to the global feedback, the partitioning of surface warming between the tropics and the southern extratropics is a key determinant of the spread in the global LR and WV feedbacks. It is also shown that model Antarctic sea ice climatology influences sea ice area changes and southern extratropical surface warming. As a result, model discrepancies in climatological Antarctic sea ice area have a significant impact on the intermodel spread of the global LR and WV feedbacks.

1. Introduction

The key features of the tropospheric warming response to increased greenhouse gas concentrations have long been understood from pioneering simulations performed with general circulation models (GCMs; Manabe and Wetherald 1975). In the tropics, where moist convection is the dominant process in setting the lapse rate, atmospheric warming largely follows a moist adiabat, which leads to amplified temperature change aloft relative to the surface (Manabe and Stouffer 1980; Santer et al. 2005). At high latitudes, where the atmosphere is stable, warming is largely confined to the lower troposphere (Manabe and Wetherald 1975; Screen et al. 2012). Arctic surface warming greatly exceeds global average surface temperature change—a phenomenon

Denotes content that is immediately available upon publication as open access.

Corresponding author: Stephen Po-Chedley, pochedley1@llnl.gov

DOI: 10.1175/JCLI-D-17-0674.1

known as Arctic amplification (e.g., Manabe and Stouffer 1980; Holland and Bitz 2003; Serreze and Francis 2006). In contrast, surface warming over the subantarctic region is muted in transient warming simulations (Stouffer et al. 1989; Manabe et al. 1991) because of circumpolar upwelling of nonequilibrated waters from depth (Armour et al. 2016). These characteristic atmospheric responses are seen both in observations and in GCM simulations forced with increasing greenhouse gas concentrations (Fu et al. 2004; Hartmann et al. 2013; Santer et al. 2013; Po-Chedley et al. 2015; Stouffer and Manabe 2017).

The horizontal and vertical structure of tropospheric warming is an important component of greenhouse gas–induced climate change. Tropospheric warming represents a fundamental climate feedback, the temperature feedback, which can be decomposed into vertically uniform (Planck feedback) and nonuniform (lapse rate feedback) constituents. Enhanced warming in the tropical upper troposphere increases longwave emission to space, leading to a negative tropical lapse rate (LR) feedback that acts to damp global temperature change under climate forcing (Hansen et al. 1984; Colman 2001; Bony et al. 2006). In regions where surface warming exceeds upper-tropospheric warming, such as in the Arctic, the LR feedback is positive (e.g., Ramanathan 1977; Schlesinger and Mitchell 1987; Colman 2001; Crook et al. 2011; Armour et al. 2013; Atwood et al. 2016; Feldl et al. 2017b). As a result, the LR feedback is a primary contributor to Arctic amplification (Pithan and Mauritsen 2014). Furthermore, it has been shown that the LR feedback interacts with the albedo feedback such that the two processes amplify one another, which in turn influences changes in atmospheric poleward heat transport (Graversen et al. 2014; Feldl and Bordoni 2016; Feldl et al. 2017a).

An important feedback that is closely related to the lapse rate feedback is the water vapor (WV) feedback (Cess 1975; Hansen et al. 1984). Tropospheric water vapor is a strong greenhouse gas, and increases in water vapor concentration with warming represent the largest positive climate feedback. To first order, atmospheric moistening follows the Clausius–Clapeyron relation (Soden and Held 2006). In the tropics, warming largely follows a moist adiabat such that warming and moistening are largest in the upper troposphere, where outgoing radiation is most sensitive to temperature and humidity perturbations (e.g., Held and Soden 2000; Soden and Held 2006). The tropics therefore strongly contribute to the individual global LR and WV feedbacks, but the net contribution of the tropics is much weaker when the feedbacks are combined (e.g., Colman 2001; Soden and Held 2006; Bony et al. 2006). The physical connection between LR and WV feedbacks suggests that they should be analyzed together when considering sources of intermodel spread in feedback strength.

On a global scale, GCMs exhibit a large range of global average surface temperature responses when forced with the same increases in greenhouse gas concentrations (e.g., Flato et al. 2013). Uncertainties in projected warming are largely due to uncertainties in the climate feedbacks that amplify or damp the initial radiative response (Colman 2001; Dufresne and Bony 2008; Caldwell et al. 2016). We define the climate feedback λ as the area-average radiative response $\Delta\overline{R}$ resulting from a given feedback process divided by the area-average surface temperature change $\Delta\overline{T}$:

$$\lambda = \frac{\Delta\overline{R}}{\Delta\overline{T}}, \tag{1}$$

where the overbar denotes area-weighted spatial averaging. This formulation can be used to define local and regional feedbacks when feedbacks are considered over a nonglobal domain (e.g., the tropics). A conventional metric for intermodel comparison is the global effective feedback λ_{eff}, defined here using the global average radiative and surface temperature change:

$$\lambda_{\text{eff}}(t) = \frac{\Delta\overline{R}_{\text{global}}(t)}{\Delta\overline{T}_{\text{global}}(t)}. \tag{2}$$

Although we largely focus on intermodel differences in the long-term, time-averaged lapse rate and water vapor feedbacks, global effective feedbacks do exhibit changes over time t (Winton et al. 2010; Armour et al. 2013; Andrews et al. 2015; Rose and Rayborn 2016; Armour 2017; Proistosescu and Huybers 2017).

The effective global LR feedback $\lambda_{\text{lr,eff}}$ and the effective global WV feedback $\lambda_{\text{wv,eff}}$ are highly variable across models. Soden and Held (2006) showed that, in the global average, models tend to moisten at approximately constant relative humidity, such that $\lambda_{\text{lr,eff}}$ covaries with $\lambda_{\text{wv,eff}}$ across models (Soden and Held 2006; Fig. 1a). Even though these feedbacks tend to cancel one another, the sum of $\lambda_{\text{lr,eff}}$ and $\lambda_{\text{wv,eff}}$ still accounts for approximately one-third of the multimodel global mean surface warming response to increases in carbon dioxide, and is an important component of the spread in climate sensitivity (Dufresne and Bony 2008; Vial et al. 2013). The LR and WV feedbacks also have physical and statistical connections to the cloud feedback, which is the primary driver of intermodel differences in climate sensitivity (Ramanathan 1977; Zelinka and Hartmann

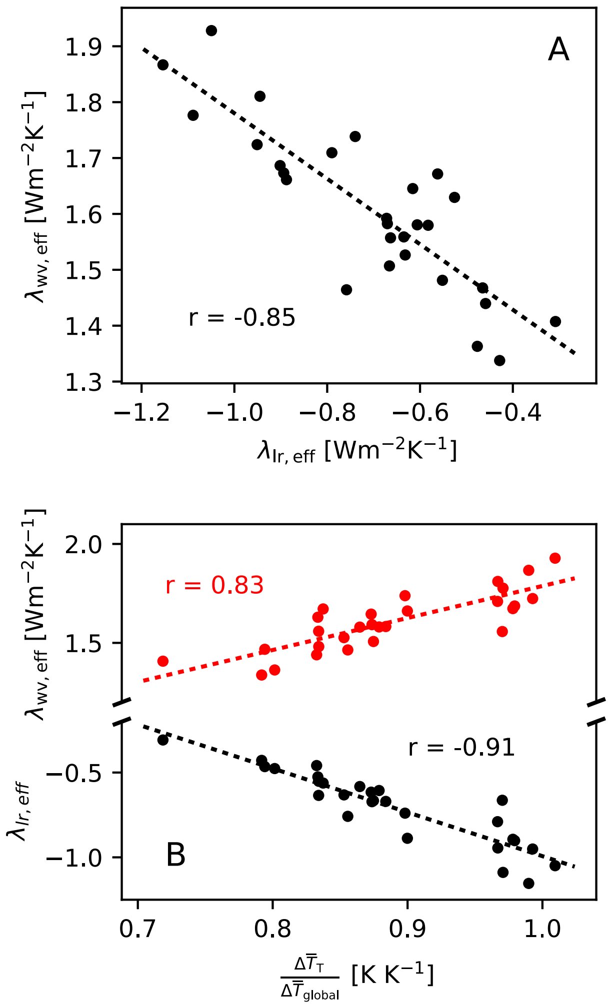

FIG. 1. (a) Global effective WV feedback vs the global effective LR feedback for each CMIP5 model analyzed here. (b) The global effective LR (black) and WV (red) feedbacks vs the ratio of tropical to global mean surface warming for each model. Note that there is a discontinuity in the y axis in (b).

2010; Mauritsen et al. 2013; Caldwell et al. 2016; Zhou et al. 2016).

One framework for interpreting climate feedbacks is that the local top-of-the-atmosphere (TOA) radiative response is assumed to depend on local surface warming (Armour et al. 2013; Feldl and Roe 2013; Roe et al. 2015), leading to a local feedback [$\lambda(r) = \Delta R(r)/\Delta T(r)$]. In this view, the local Planck feedback has the useful property of being near constant across models and over time, but varying spatially primarily because of the temperature dependence of blackbody radiation (Feldl and Roe 2013; Feldl et al. 2017b). Differences in the warming pattern over time or across models can then modulate the strength of the effective global average feedback via the following relationship (Armour et al. 2013):

$$\lambda_{\text{eff}}(t) = \overline{\lambda(r,t)\frac{\Delta T(r,t)}{\Delta \overline{T}_{\text{global}}(t)}}, \tag{3}$$

where the overbars represent spatial averaging over the globe. Equation (3) represents the activation of spatially dependent local feedbacks by a particular pattern of surface warming, where λ could in principle depend on both space and time (Rose et al. 2014; Andrews et al. 2015). It is also possible that individual GCMs may differ in their representation of local feedback processes. For example, differences in the way in which models parameterize deep convection could result in tropical feedbacks that differ across models.

Soden and Held (2006) found the intriguing result that the global LR and WV feedbacks are strongly related to the ratio of tropical to global surface warming (Fig. 1b). However, the physical basis for this finding is not yet fully understood. One plausible interpretation in terms of local feedbacks is as follows: Because the tropical troposphere is convectively coupled to the tropical ocean surface, warming of the tropical ocean surface leads to enhanced upper-tropospheric warming and moistening and a negative (positive) local LR (WV) feedback. Since the global effective feedbacks are normalized by the global average surface temperature, models with a larger ratio of tropical to global surface warming exhibit stronger LR and WV feedbacks. It is also possible, however, that local lapse rate and water vapor changes, and their associated feedbacks, may depend on the spatial pattern of surface warming itself. Indeed, several studies have shown that local feedbacks depend on nonlocal processes, such as the collocation of warming with tropical deep convection (Flannaghan et al. 2014; Ferraro et al. 2015; Zhou et al. 2016; Po-Chedley 2016) and poleward atmospheric heat transport (Payne et al. 2015; Cronin and Jansen 2016). In contrast to the tropical vertical temperature profile, which is largely set by radiative–convective equilibrium, the high-latitude vertical temperature profile is set by radiative–advective equilibrium (Payne et al. 2015). In these regions, the vertical profile of warming and moistening is dependent both on surface processes (e.g., albedo changes) as well as on tropospheric warming that arises in part from poleward heat transport. In this case, it is important to identify and understand nonlocal influences on regional feedbacks.

A key question is then, what sets the magnitude of the global LR and WV feedbacks and their variation across models? On one hand, they could be primarily driven by variations in the pattern of surface warming activating regions of differing feedback strengths; on the other hand, it could be the pattern of surface warming itself contributing nonlocally to the magnitude of the locally defined LR and WV feedbacks. Alternatively, different approaches in parameterizing subgrid processes, such as convection, may also be important. Here we quantify these sources of variation in the global LR and WV feedbacks across an ensemble of climate models by analyzing the principal patterns of feedback variability under CO_2 forcing.

2. Data

The models considered in our study are from phase 5 of the Coupled Model Intercomparison Project (CMIP5; Taylor et al. 2012). We compare the response of models forced with an abrupt quadrupling of carbon dioxide (abrupt4xCO2 experiment) to control simulations with a constant preindustrial CO_2 concentration (piControl simulation). The climate radiative feedback fields used in this study are from Caldwell et al. (2016). Caldwell et al. (2016) used the difference between each model's abrupt4xCO2 experiment and the contemporaneous 21-yr running mean from the piControl simulation for feedback calculations. Feedbacks are calculated using all-sky radiative kernels from Soden et al. (2008). Radiative kernels represent the TOA radiative response (i.e., ∂R) to atmospheric and surface state perturbations (i.e., ∂x). The radiative kernel $\partial R/\partial x$ can then be multiplied by the warming response (i.e., dx) of a given state variable (e.g., temperature and water vapor) to estimate the radiative impact of its changes. As discussed above, the global effective feedback is the global radiative response normalized by global mean surface warming [Eq. (2)]. The temperature and water vapor kernels used in this assessment (Soden et al. 2008) are included as Fig. 2 for reference.

To aid in interpreting the intermodel spread in the LR and WV feedbacks, we also analyze changes in CMIP5 near-surface air temperature (tas), atmospheric temperature (ta) and humidity (hus), and sea ice concentration (sic). All fields considered in this study are from each model's r1i1p1 realization. Unless otherwise noted, the perturbed fields and feedbacks are calculated using the annual average response 120–140 years after CO_2 quadrupling, which effectively removes the influence of year-to-year variability on the results presented here. Caldwell et al. (2016) determine the global feedbacks by regressing the radiative changes against global temperature, whereas we simply divide the radiative change by the surface temperature change [Eq. (1)]. The results are expressed relative to the contemporaneous segment of the piControl simulation. Since we utilize the feedback calculations from Caldwell et al. (2016), we consider the same 28 models. We also make use of the European Centre for

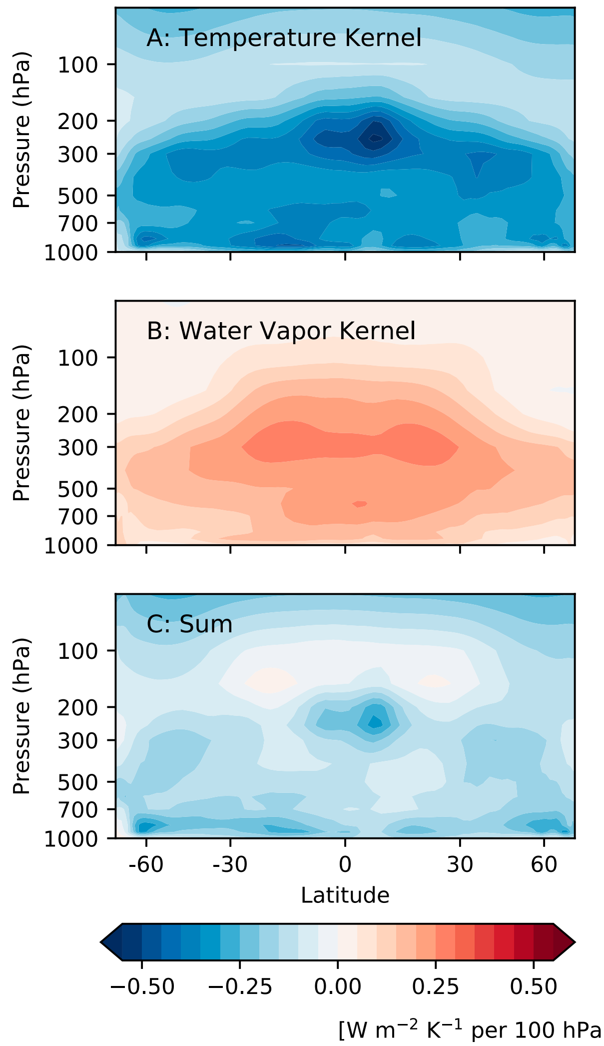

FIG. 2. Zonal mean radiative kernels for (a) temperature, (b) WV, and (c) the sum of (a) and (b). The kernel represents the TOA radiative response (positive down) for a 1-K temperature perturbation. For WV, the kernel represents the sensitivity to WV changes for a 1-K temperature perturbation at constant RH. Radiative kernels are from Soden et al. (2008). Note that the x axis is scaled by the sine of the latitude, and the x-axis limits are ±90°.

Medium-Range Weather Forecasts (ECMWF) interim reanalysis (ERA-I) product to estimate observationally based trends and variability in atmospheric temperature and humidity since 1979 (Dee et al. 2011).

As noted above, a number of previous studies have summed the LR and WV feedback into one term, which has reduced intermodel spread compared to the individual LR and WV feedbacks (e.g., Colman 2003; Soden and Held 2006). Held and Shell (2012) used the sum of the temperature radiative kernel (the longwave effect of a 1-K temperature perturbation) and the water vapor radiative kernel (the longwave and shortwave effect of water vapor for a 1-K temperature increase assuming constant relative humidity) to calculate a lapse rate feedback that includes the influence of water vapor at constant relative humidity (denoted as $\tilde{\lambda}_{\rm lr}$). The sum of the temperature and water vapor kernels is also included in Fig. 2. In the Held and Shell (2012) partitioning, changes in moisture associated with vertically uniform warming are included in the Planck feedback, and changes in moisture associated with deviations from vertically uniform warming are a part of the lapse rate feedback. The contribution from changes in relative humidity (RH) are expressed separately as the RH feedback $\tilde{\lambda}_{\rm rh}$. On regional scales, changes in relative humidity can be important, particularly in the tropics and subtropics (O'Gorman and Muller 2010). Radiative effects of temperature and humidity changes expressed in the traditional feedback framework ($\lambda_{\rm lr,eff} + \lambda_{\rm wv,eff}$) strongly covary ($r = 0.95$) with corresponding results from the Held and Shell (2012) constant-RH framework ($\tilde{\lambda}_{\rm lr,eff} + \tilde{\lambda}_{\rm rh,eff}$), and the two definitions have nearly identical intermodel variance. The two sets of definitions have different absolute values, however, because Held and Shell (2012) include the radiative effects of the moistening associated with vertically uniform warming in the Planck feedback.

Model differences in the simulation of relative humidity changes may relate to the simulation of moisture transport (Sherwood et al. 2010), although some analytical theories relate relative humidity changes to humidity climatology (Singh and O'Gorman 2012; Romps 2014). We primarily use the Held and Shell (2012) formulation to separate the effects of lapse rate changes at constant relative humidity $\tilde{\lambda}_{\rm lr}$ and changes in relative humidity $\tilde{\lambda}_{\rm rh}$, although some results are also presented in terms of the conventional LR $\lambda_{\rm lr}$ and WV $\lambda_{\rm wv}$ feedbacks.

3. Variability in the local lapse rate and water vapor feedbacks

Under the framework given in Eq. (3), the global effective feedback is a function of both the pattern of local climate feedbacks and the pattern of surface warming. Model differences in the global effective feedback can arise from either term. To examine the geographic regions in which models differ from one another, we show both terms in Fig. 3. The zonally averaged LR and WV feedbacks (i.e., the zonal mean radiative change resulting from LR and WV changes divided by the zonal mean surface temperature change) tend to have small intermodel spread at most latitudes, except in the subantarctic region, where models tend to disagree substantially (Figs. 3a,b). The sum of the LR and WV feedbacks also show large spread in this region (Fig. 3c). These results suggest that the Southern Ocean may be important in understanding the intermodel spread in the global effective LR and WV feedbacks.

Using the Held and Shell (2012) definition of the lapse rate feedback at constant relative humidity, we find a similar result: Most of the model disagreement in the local feedback is concentrated in the subantarctic region (Fig. 3d). In contrast, the intermodel spread in the relative humidity feedback is largest in the tropics, with relatively little spread in the extratropics, as suggested by Vial et al. (2013) (Fig. 3e). The common intermodel variability in the LR and WV feedbacks over the subantarctic region suggests model disagreement in this region may be caused by the same physical mechanism. Further, since relative humidity contributions to the feedbacks are small in the extratropics, $\tilde{\lambda}_{\rm lr}$ is representative of the sum of the LR and WV feedbacks ($r = 0.99$). In addition to these features of the spread in the individual feedbacks, there is also substantial intermodel spread in the pattern of warming over polar and subpolar regions (Fig. 3f). As noted in the introduction, models tend to have a minimum in warming over the subantarctic region and a maximum in warming over the Arctic.

Next, we explore possible drivers of the intermodel spread in the magnitude of local feedbacks over the subantarctic region. Several studies have pointed out that the pattern of surface warming can have nonlocal effects. Flannaghan et al. (2014) showed that preferential sea surface warming in the tropical Pacific warm pool results in enhanced upper-tropospheric warming throughout the tropics. Similarly, Butler et al. (2010) showed that a heating source in the tropical upper troposphere tends to warm the midlatitude troposphere. Screen et al. (2012) also found that the remote influence of the tropics is critical to reproducing the observed vertical and seasonal warming in the Arctic. Other work has also shown that warming over high latitudes can have a similar nonlocal effect (e.g., Roe et al. 2015; Deser et al. 2016). In contrast, several studies indicate that a heating source applied in the polar lower troposphere leads to warming that is largely confined to the near surface in the middle and high latitudes (Butler et al. 2010; Laliberté and Kushner 2013). These studies analyzed the patterns of atmospheric warming associated with various patterns of heating or sea surface temperature changes within a particular set of models.

We find similar sets of patterns looking across the 28 CMIP5 models considered here. In Fig. 4, we show the zonal mean atmospheric warming pattern associated with southern extratropical (Fig. 4a; 30°–90°S), tropical (Fig. 4b; 30°S–30°N), and northern extratropical (Fig. 4c; 30°–90°N) surface warming. Specifically, we contour the

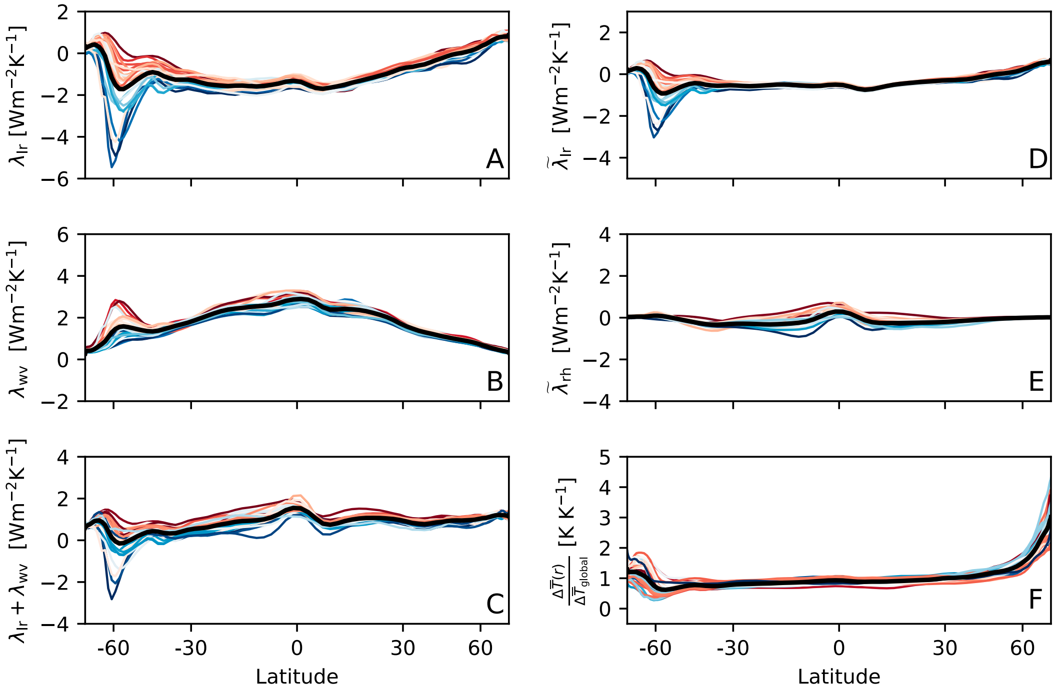

FIG. 3. The zonal average local feedbacks for (a) LR λ_{lr}, (b) WV λ_{wv}, (c) the sum of LR + WV, (d) constant-RH LR $\tilde{\lambda}_{lr}$, and (e) RH λ_{rh}. Results are for all 28 models (colored lines). (f) The zonal mean surface warming normalized by the model's global average surface warming. In each panel, the colors correspond to different values of the global effective feedback, ranging from low (dark blue) to high values (bright red). The multimodel average is indicated by a solid black line. For (f), the colors correspond to different model values of global average surface warming. Note that the x axis is scaled by the sine of latitude, the x-axis limits are $\pm 90°$, and the y-axis ranges are the same in (a)–(e).

slope of the linear relationship between zonal mean atmospheric warming (28 GCM predictands at each point) and area-averaged surface warming (28 GCM predictors) across models (hatching denotes a relationship that is statistically significant at the 5% level or better). In the models analyzed here, enhanced tropical upper-tropospheric warming that extends through the midlatitudes is related to tropical surface warming (Fig. 4b). Models with larger surface warming in the southern extratropics tend to be associated with polar amplification of warming that is largest and most significant in the SH lower troposphere (Fig. 4a). A similar pattern emerges in the northern extratropics. Since surface warming in the northern extratropics is significantly related to surface warming in the tropics (r = 0.72 across the 28 CMIP5 models), the statistical significance of the response in the tropical troposphere is more pronounced in Fig. 4c. The relationship between surface warming in the tropics and southern extratropics is much weaker (r = 0.42). A likely explanation for this asymmetric behavior is that heat fluxes in the Southern Ocean are largely balanced by ocean heat transport associated with equatorward flow of surface waters (Marshall et al. 2015; Armour et al. 2016). As a result, southern extratropical surface warming, in the subantarctic region in particular, is relatively insensitive to enhanced atmospheric poleward heat fluxes associated with tropical warming. In the northern extratropics, where the ocean does not compensate for atmospheric poleward heat flux, surface warming is more sensitive to the remote influence of the tropics (Screen et al. 2012; Marshall et al. 2015; Ding et al. 2017).

Similar relationships between surface and atmospheric temperature also appear using observational reanalysis products. In Fig. 4, we use ERA-I for the period 1979–2016 to regress the regional average, annual-mean surface temperature in the southern extratropics (Fig. 4d), tropics (Fid. 4e), and northern extratropics (Fig. 4f) against atmospheric temperature. In producing Figs. 4d–f, the reanalysis data are not detrended, but we obtain qualitatively similar results when we detrend both the surface temperature and atmospheric time series (not shown). The patterns derived from interannual variations in ERA-I broadly match those from intermodel differences in CMIP5 data. Differences between the two analyses are likely the result of

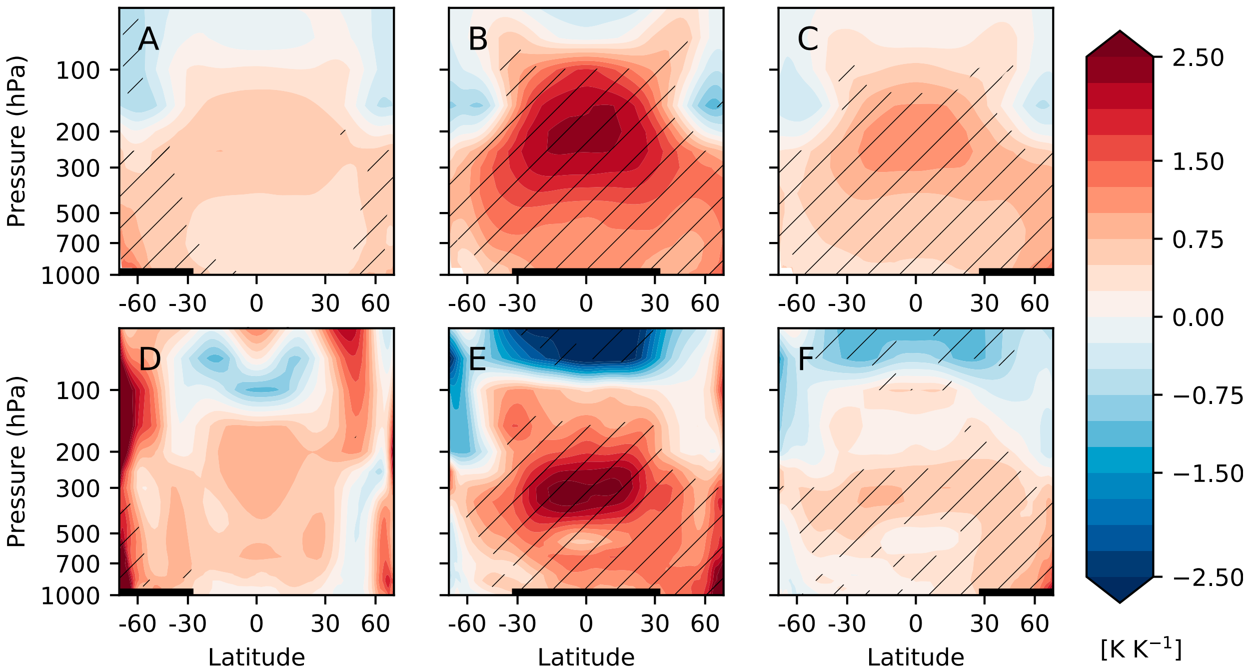

FIG. 4. The slope of the regression between zonal mean atmospheric warming and (a) southern extratropical (30°–90°S), (b) tropical (30°S–30°N), and (c) northern extratropical (30°–90°N) average surface warming across models. The thick lines at the surface represent the region over which the predictor is averaged. The hatch marks denote a significant relationship at the 95% confidence level. The regression is for annual average surface temperature in the (d) southern extratropics, (e) tropics, and (f) northern extratropics vs annual- and zonal-mean atmospheric temperature in ERA-I (1979–2016). Note that the *x* axis is scaled by the sine of latitude, and the *x*-axis limits are ±90°.

differences between the observed and abrupt4xCO2 forcing, natural variability, and time-varying inhomogeneities in the global observing system (e.g., Thorne 2008; Thorne and Vose 2010; Fu et al. 2011; Po-Chedley and Fu 2012; Santer et al. 2014; Bandoro et al. 2014). This suggests that broad, coherent patterns of atmospheric warming are associated with relatively simple metrics—area-averaged surface warming—and that these features are apparent across GCMs and over time in the observational record.

In Fig. 5, we show a similar analysis but for fractional changes in atmospheric humidity. The most prominent feature is that models with greater tropical surface warming strongly humidify the tropical upper troposphere (Fig. 5b). This is due to the combined effect of two factors: vertical amplification of warming with height (e.g., Santer et al. 2005; Fig. 4b) and because the Clausius–Clapeyron scaling is greater for temperature changes in the cold upper troposphere (e.g., Rose and Rencurrel 2016). The upper troposphere in the extratropics also experiences significant increases in water vapor content in models with enhanced tropical surface warming. In the case of southern extratropical surface warming (Fig. 5a) atmospheric humidification is relatively weak and is largely isolated to the Southern Hemisphere. In contrast, greater northern extratropical surface warming corresponds to significant global humidification in CMIP5 models, probably as a result of the above-mentioned correlation between tropical and northern extratropical surface warming.

Analysis using ERA-I broadly shows similar features (Figs. 5d–f). As in the case of the temperature results in Fig. 4, some differences exist between the analysis using CMIP5 models and ERA-I, particularly in the vertical extent and significance of upper-tropospheric moistening. This is likely due in part to inhomogeneities in the reanalysis record (e.g., Bengtsson et al. 2004). Upper-tropospheric water vapor trends are quite uncertain, are sensitive to changes in the global weather observing system, and can be difficult to observe directly (e.g., Elliott and Gaffen 1991; Bengtsson et al. 2004; Dessler and Davis 2010).

Because the vertical and meridional patterns of atmospheric warming and moistening are closely related to the magnitude of surface warming in the tropics and the extratropics, it may be possible to estimate the expected TOA radiative effect of lapse rate and water vapor changes using area-average surface warming as a predictor. Consider the following example. To a first order, the tropical troposphere experiences moist adiabatic warming and moistening as a function of surface temperature change. Since the profile of temperature

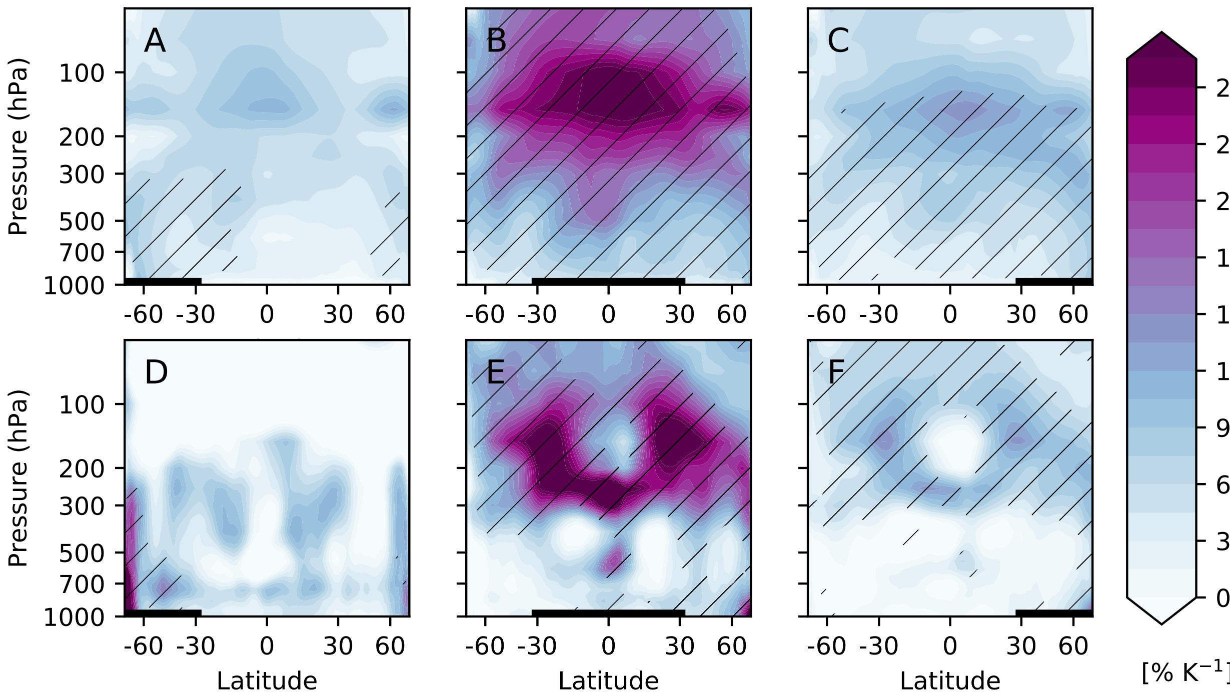

FIG. 5. As in Fig. 4, but for the fractional change in humidity (i.e., $\partial \log q$).

and water vapor changes determines the TOA radiative change as calculated from radiative kernels, the tropical radiative change resulting from lapse rate and water vapor changes is a function of tropical surface temperature change. We then write the tropical radiative change as

$$\Delta \overline{R}_T = c\Delta \overline{T}_T, \quad (4)$$

where $\Delta \overline{R}_T$ is the tropical average radiative flux change as a result of lapse rate and/or water vapor changes, c is a scaling coefficient, and $\Delta \overline{T}_T$ is the tropical average surface warming. We will use a tilde in place of overbars to denote radiative flux changes that occur at constant relative humidity (e.g., $\Delta \tilde{R}$). Similarly, extratropical upper-tropospheric warming and moistening is strongly influenced by tropical surface warming $\Delta \overline{T}_T$ (Figs. 4 and 5b,e), and changes in the lower extratropical troposphere are related to the extratropical surface warming $\Delta \overline{T}_{\mathrm{ET}}$. We express the extratropical radiative flux as

$$\Delta \overline{R}_{\mathrm{ET}} = a\Delta \overline{T}_{\mathrm{ET}} + b\Delta \overline{T}_T, \quad (5)$$

where a and b are scaling coefficients and the subscript ET can denote either the northern (denoted with subscript N) or southern (denoted with subscript S) extratropics (30°–90°). These equations could be applied toward radiative fluxes associated with either the regional LR, WV, or the constant-RH LR feedbacks. The scaling coefficients in Eqs. (4) and (5) are physically related to the sensitivity of TOA radiative flux associated with the change in temperature and moisture (i.e., the radiative kernel; Fig. 2) and the patterns of warming and moistening associated with tropical and extratropical surface warming (Figs. 4 and 5). We will solve for these coefficient values using linear regression. Specifically, we solve for c in Eq. (4) by regressing $\Delta \overline{R}_T$ against $\Delta \overline{T}_T$ across CMIP5 GCMs. In Eq. (5), we solve for a and b using multiple linear regression.

These simple linear models can explain most of the intermodel differences in the radiative fluxes arising from lapse rate and water vapor changes. For example, GCM tropical radiative fluxes resulting from lapse rate and water vapor changes at constant relative humidity are simply a function of tropical surface warming, with a scaling coefficient of $c = -0.52\,\mathrm{W\,m^{-2}\,K^{-1}}$ [Fig. 6a, $r^2 = 0.84$; Eq. (4)]. The GCM radiative fluxes averaged over the northern (red) and southern (blue) extratropics also scale closely with the fluxes expected from our simple linear model [Fig. 6b, $r^2 = 0.95$; Eq. (5)]. For both the tropical and extratropical cases, a good fit is obtained with the y intercept equal to zero, which suggests that the effect of the fast tropospheric adjustments to forcing (e.g., Gregory and Webb 2008; Andrews and Forster 2010) on lapse rate and water vapor changes is small.

In this analysis, we are particularly interested in the radiative feedbacks, which are the average radiative flux

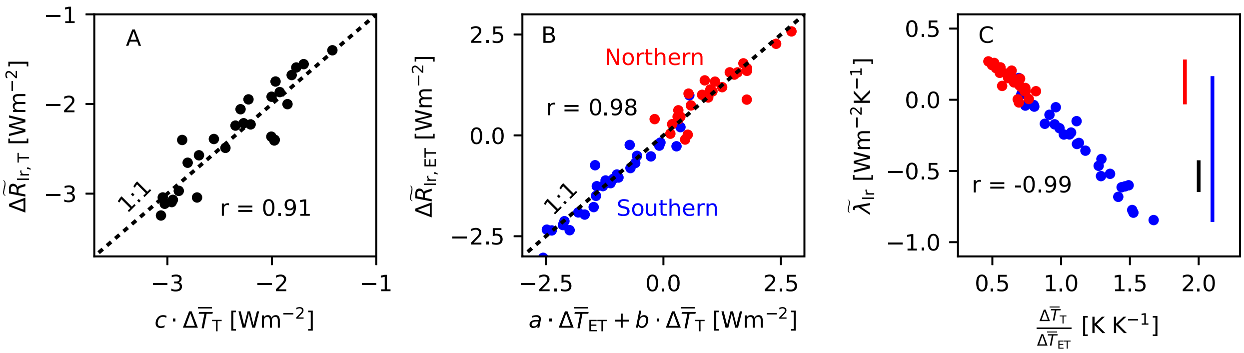

FIG. 6. (a) Radiative flux change resulting from LR and WV changes at constant RH; results for each model are averaged over the tropics (30°S–30°N), and are plotted against the linear model of tropical radiative flux change given in Eq. (4) (the sign convention is such that positive is downward, so negative anomalies imply an increase in outgoing radiation). (b) Model radiative flux change resulting from LR and WV changes at constant RH averaged over the extratropics (30°–90°); results are given separately for the Northern (red) and Southern (blue) Hemisphere, and are compared to a linear model of the extratropical radiative flux change [Eq. (5)]. The 1:1 line is shown for reference in (a) and (b). The linear models use $a = 0.71$, $b = -0.90$, and $c = -0.52\ \mathrm{W\,m^{-2}\,K^{-1}}$. (c) Model $\tilde{\lambda}_{\mathrm{lr}}$ in the northern (red) and southern (blue) extratropics vs the ratio of each model's tropical and extratropical average warming. The domain is over 30°–90°N in the Northern Hemisphere and 30°–90°S in the Southern Hemisphere. The vertical lines in this panel represent the range of the model tropical (black), northern extratropical (red), and southern extratropical (blue) constant-RH LR feedbacks.

per unit surface warming [Eq. (1)]. For the tropics, this means that [from Eq. (4)]

$$\lambda_T = \frac{\Delta\overline{R}_T}{\Delta\overline{T}_T} = c, \qquad (6)$$

which implies that the tropical LR and WV feedbacks are approximately constant. Similarly, for the extratropics [from Eq. (5)]

$$\lambda_{\mathrm{ET}} = a + b\frac{\Delta\overline{T}_T}{\Delta\overline{T}_{\mathrm{ET}}}, \qquad (7)$$

indicating that the model variability for the extratropical LR and WV feedbacks should scale with the ratio of tropical and extratropical surface warming. This result is consistent with past work that has shown that the extratropical lapse rate is constrained by baroclinic adjustment (Stone 1978; Bony et al. 2006) and that changes in the meridional temperature gradient correspond to changes in dry static stability (Frierson 2006, 2008). We demonstrate that this scaling holds for $\tilde{\lambda}_{\mathrm{lr}}$ in Fig. 6c ($r^2 = 0.97$). In Fig. 6c, we also show the intermodel feedback spread in the tropics (black vertical line) and the northern (red) and southern (blue) extratropics. As expected from Eq. (6), the tropical feedback is nearly constant ($\tilde{\lambda}_{\mathrm{lr},T} = -0.52$ and the standard deviation σ is 0.05). Note that the regional feedback scalings shown for Fig. 6 also work for the conventional lapse rate (see Fig. A1 in the appendix) and water vapor feedback (see Fig. A2 in the appendix). The success of these scalings demonstrates that it is largely patterns of warming that control the radiative response as a result of lapse rate and water vapor changes, not differences in individual models' physical parameterizations. We have highlighted $\tilde{\lambda}_{\mathrm{lr}}$ because the intermodel spread in the local LR and WV feedbacks is largest in the extratropics, where changes in relative humidity are small (Fig. 3e). Therefore, $\tilde{\lambda}_{\mathrm{lr}}$ represents the bulk of the extratropical LR and WV feedback variability among models.

While the global LR and WV feedbacks show strong covariability across models (Fig. 1a), the local feedback perspective can shed light on the physical connections between these feedbacks. In the extratropics, the LR feedback is closely tied to the ratio of tropical to extratropical surface warming [Eq. (7); Fig. A1]. Since relative humidity changes are small in the extratropics (Fig. 3e), the extratropical water vapor feedback is largely controlled by the vertical profile of warming, and thus should be closely coupled with the LR feedback. As a result, the strength of both feedbacks is highly correlated in the extratropics (30°–90°, Fig. 7a). In the tropics, the LR and WV feedbacks are only weakly correlated across models (Fig. 7a), even though the regional LR and WV feedbacks are largest in the tropics and both feedbacks, to a first order, stem from the moist adiabatic warming (and moistening) response of the tropical atmosphere. Vial et al. (2013) showed that the sum of the tropical LR and WV feedbacks is closely related to GCM changes in relative humidity. We find that this relation is largely driven by the strong correlation between the tropical WV and RH feedback (Fig. 7b); the tropical LR feedback is uncorrelated with the RH feedback ($r = 0.03$). This implies that although

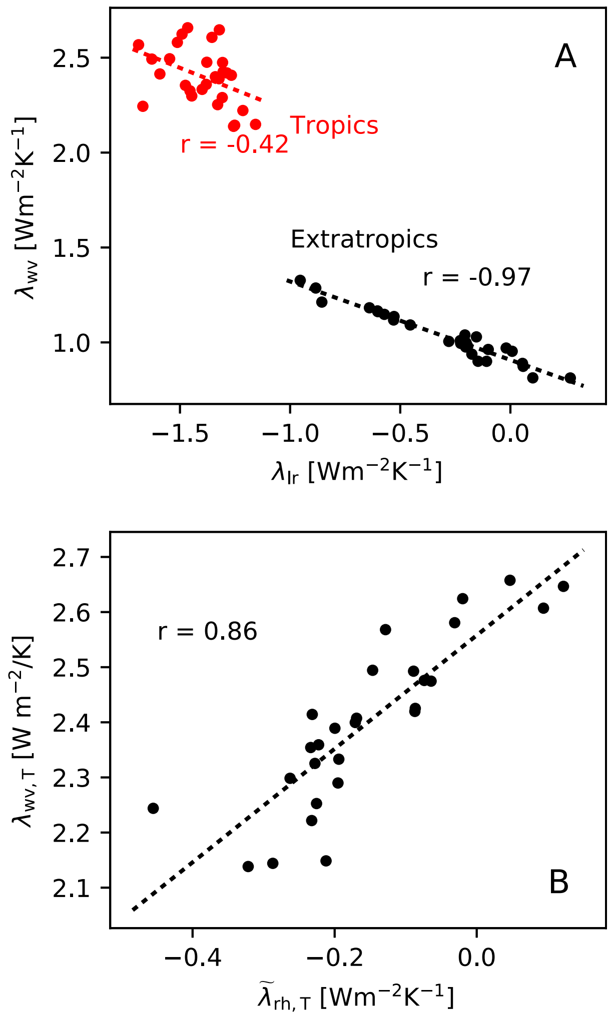

FIG. 7. (a) The WV feedback vs the LR feedback in the tropics (30°S–30°N; red) and the extratropics (30°–90°; black) for each model. (b) The tropical WV feedback vs the tropical RH feedback for each model.

the first-order response to tropical surface temperature increase is moist adiabatic warming and moistening, the intermodel differences in the water vapor feedback are controlled by relative humidity changes. In turn, the tropical RH changes have no physical link to the model lapse rate response, which is largely constant across models [Eq. (6); Fig. A1]. The coupling between the tropical LR and WV feedbacks across models is therefore weak.

An obvious asymmetry exists for the spread in the local LR and WV feedbacks in the northern and southern extratropics (Figs. 3 and 6c). The standard deviation of $\tilde{\lambda}_{lr}$ in the southern extratropics is roughly 3 times larger than that in the northern extratropics (σ_S = 0.27 vs σ_N = 0.08). From Eq. (5), we expect that extratropical radiative fluxes as a result of lapse rate and water vapor changes should partially scale with extratropical surface warming. In Fig. 8a, we see that this expectation holds; models with greater extratropical surface warming have larger extratropical radiative fluxes (positive down). There is, however, substantial scatter around the linear fit because Fig. 8a ignores the effects of surface warming in the tropics [Eq. (5)]. The y intercept can be interpreted as the nonlocal effect on the lapse rate changes; when extratropical surface warming approaches zero, the radiative fluxes are negative as a result of the remote influence of the tropics (Figs. 4b and 5b). Although here we emphasize a nonlocal influence in the meridional direction, tropical feedbacks also respond to east–west warming gradients. Enhanced warming in the tropical warm pool increases atmospheric stability in the eastern Pacific, which results in a strong negative cloud and lapse rate feedback (Flannaghan et al. 2014; Ferraro et al. 2015; Zhou et al. 2016; Andrews and Webb 2018; Ceppi and Gregory 2017).

This nonlocal effect is particularly important when calculating feedbacks. The regional average feedback is simply the area-averaged radiative flux normalized by the area-averaged surface warming (i.e., $\tilde{\lambda}_{lr} = \Delta\tilde{R}_{lr}/\Delta\overline{T}$), which we show as a function of extratropical surface warming in Fig. 8b. An apparent nonlinearity in the extratropical constant-RH LR feedback occurs with respect to extratropical surface warming. When surface warming is small, the magnitude of the feedback grows quite large [as $\Delta\overline{T}_{ET} \to 0$ and $\tilde{\lambda}_{lr,ET} \to -\infty$ from Eq. (7)]. This has an important effect in the Southern Hemisphere, where the amplitude of surface warming is relatively small compared to the Northern Hemisphere (Fig. 3f). The curvature in Fig. 8b results in a larger spread in the LR and WV feedbacks in the southern extratropics relative to the northern extratropics.

Another factor in the reduced feedback spread in the northern extratropics is the large correlation between tropical and northern extratropical surface warming (r = 0.72). This reduces the spread in the ratio $\Delta\overline{T}_T/\Delta\overline{T}_N$, which is a key determinant of extratropical LR and WV feedbacks (Figs. 6c, A1c, and A2c). The physical interpretation of this result is that extratropical upper-tropospheric warming and moistening is closely tied to tropical surface warming, whereas extratropical lower-tropospheric warming is related to extratropical surface warming. Since tropical and northern extratropical surface warming are correlated across models, the relative upper- and lower-tropospheric warming and moistening in the NH, and resulting NH-averaged feedbacks, tend to exhibit reduced intermodel spread. Smaller southern extratropical surface warming and a

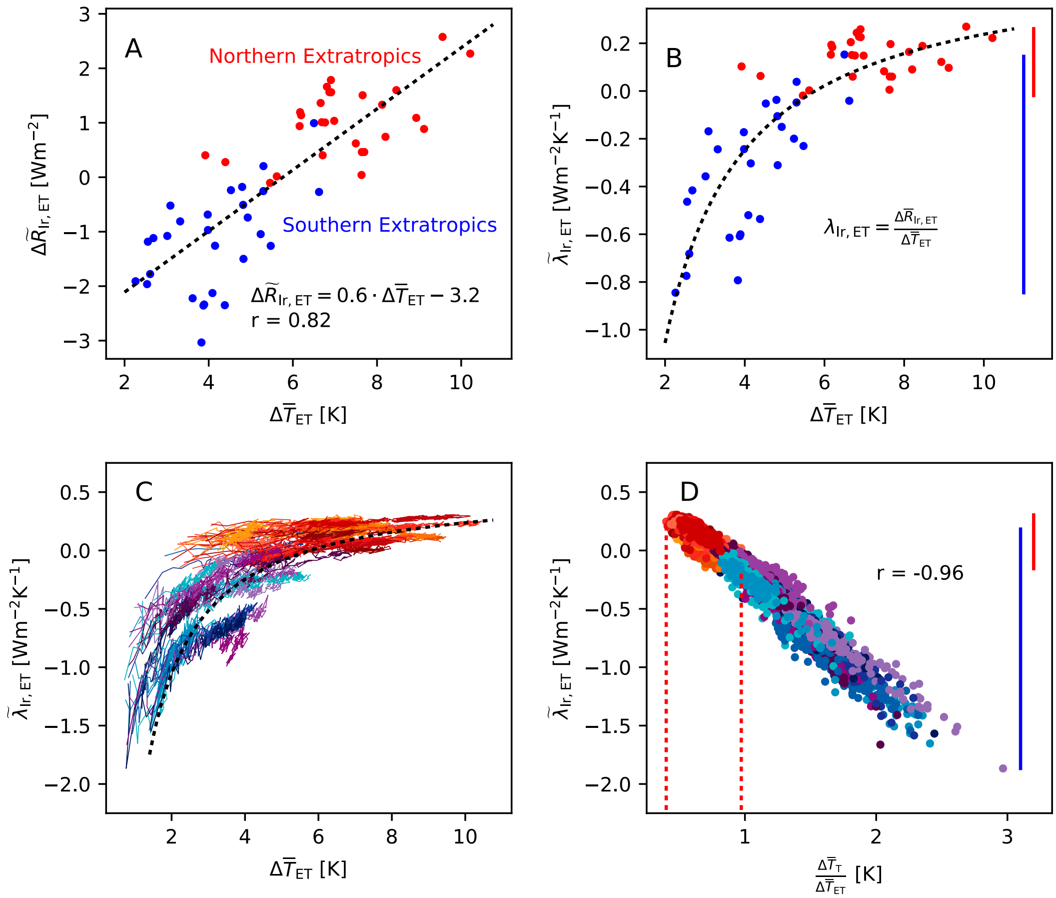

FIG. 8. (a) The extratropical (30°–90°) radiative response to LR and WV changes at constant RH vs extratropical surface warming; results are for 28 different CMIP5 models. The red dots are for the Northern Hemisphere and the blue dots are for the Southern Hemisphere. (b) As in (a), except that the relationship is between the feedback $\tilde{\lambda}_{\mathrm{lr,ET}}$ and the surface warming response. (c) Annual average local $\tilde{\lambda}_{\mathrm{lr}}$ over years 1–150 in individual GCMs vs the local surface warming in the southern extratropics (varied cool colors for each individual model time series) and the northern extratropics (varied warm colors). (d) Annual average local $\tilde{\lambda}_{\mathrm{lr}}$ over years 1–150 in individual GCMs vs the ratio of tropical (30°S–30°N) and extratropical (30°–90°) surface warming. The domains are 30°–90°N in the Northern Hemisphere and 30°–90°S in the Southern Hemisphere. The solid vertical lines in (b) and (d) help illustrate the range of the feedback values for the northern (red) and southern (blue) extratropics. The dashed line in (a) is the linear fit to all data points. The dashed line in (b) is the dashed line from (a), divided by $\Delta\overline{T}_{\mathrm{ET}}$. The dashed line in (c) is the same as the line in (b), but extended over a greater range of extratropical surface warming values. In (d) the range of the ratio of tropical and northern extratropical surface warming is represented by dashed, red vertical lines.

reduced correlation with tropical surface warming (as compared to the Northern Hemisphere) both contribute to larger model spread for the Southern Hemisphere WV and LR feedbacks. Experiments with synthetic data containing the same statistical properties as the CMIP5 model data show that reduced warming in the Southern Hemisphere is the dominant factor (more than twice as important as the relatively weak correlation between tropical and southern extratropical surface warming) in the asymmetry in the feedback spread between the northern and southern extratropics (not shown).

Although this analysis focuses on explaining intermodel differences in feedback strength, we can also apply this framework to investigate changes in model feedbacks over time. In Fig. 8c, extratropical $\tilde{\lambda}_{\mathrm{lr}}$ is plotted against extratropical surface temperature change over years 1–150 for each GCM. Results are shown separately for the Southern Hemisphere (cool colors) and the Northern Hemisphere (warm colors); all changes are expressed relative to the contemporaneous piControl simulation. From Fig. 8, we see that in the SH there is an apparent nonlinearity in the evolution of the feedback as a function of increasing warming. In contrast, the NH has relatively little curvature. The NH result occurs because across all models and all years, the ratio of warming between the tropics and NH is relatively constant, which ensures that the NH extratropical feedback has little intermodel spread.

Although this time-varying behavior is not the focus of our research, this analysis demonstrates that the same physical mechanisms identified above across 28 CMIP5 models also apply in individual model simulations, and that the evolution of $\tilde{\lambda}_{\mathrm{lr}}$ contributes to changes in climate sensitivity with warming (e.g., Rose et al. 2014; Andrews et al. 2015; Rose and Rayborn 2016; Rugenstein et al. 2016). The curvature in Figs. 8b,c is simply a result of the linear contributions from both the tropics and the extratropics to the feedback [Eqs. (5) and (7)]. If we instead show (Fig. 8d) the feedback compared to the ratio of tropical and extratropical warming (i.e., $\Delta\overline{T}_T/\Delta\overline{T}_{\mathrm{ET}}$ as in Fig. 6c), we see that the feedback is linearly proportional to this ratio [as expected from Eq. (7)]. As we noted earlier in Fig. 8c, the relatively constant scaling of tropical and northern extratropical surface warming ensures that the Northern Hemisphere lapse rate feedback is approximately constant across all models and all years (as denoted by the red vertical line in Fig. 8d). Reduced warming in the Southern Ocean and the largely uncorrelated warming between the tropics and the Southern Hemisphere makes the Southern Hemisphere extratropical lapse rate feedback highly variable (blue vertical line in Fig. 8d). A similar apparent nonlinearity also exists for the conventional LR and WV feedbacks (not shown).

Another feature of these simple linear models of local feedbacks is that we can also write an expression for the global effective feedback. Using the fact that $\Delta\overline{T}_{\mathrm{globe}} = 1/2(\Delta\overline{T}_T) + 1/2(\Delta\overline{T}_{\mathrm{ET}})$ with Eqs. (4) and (5), we can show that the global feedback can be written as

$$\lambda_{\mathrm{eff}} = a + \kappa\frac{\Delta\overline{T}_T}{\Delta\overline{T}_{\mathrm{global}}}, \tag{8}$$

where $\kappa = (b + c - a)/2$. This expression is consistent with Soden and Held (2006), who showed that the ratio of tropical and global surface warming is a strong predictor of the global effective LR and WV feedbacks (Fig. 1b). This scaling also works well for $\tilde{\lambda}_{\mathrm{lr,eff}}$ ($r = -0.92$; not shown).

4. From local to global

Recall from Eq. (3) that the global effective feedback is the product of the pattern of local feedbacks $\lambda(r)$ and the spatial pattern of surface warming $\Delta T(r)/\Delta T_{\mathrm{global}}$. Both terms may contribute to the intermodel spread in the lapse rate and water vapor feedback. We can estimate the sensitivity of the global effective feedback to both the patterns of surface warming and of local feedbacks. To estimate the sensitivity of the global effective feedback to intermodel differences in the local feedbacks, we use the multimodel average warming pattern. From Eq. (3):

$$\lambda_{\mathrm{eff}\langle\mathrm{warming\ pattern}\rangle} = \overline{\lambda(r)\left\langle\frac{\Delta T(r)}{\Delta\overline{T}_{\mathrm{global}}}\right\rangle}, \tag{9}$$

where the angle brackets denote the multimodel average. Similarly, we can use the multimodel average pattern of local feedbacks to estimate the sensitivity to intermodel differences in the surface warming pattern:

$$\lambda_{\mathrm{eff}\langle\mathrm{feedback\ pattern}\rangle} = \overline{\langle\lambda(r)\rangle\frac{\Delta T(r)}{\Delta\overline{T}_{\mathrm{global}}}}. \tag{10}$$

Equations (9) and (10) can be used to help reveal the key drivers of intermodel differences in the global effective lapse rate and water vapor feedbacks. If the global effective feedback spread is largely a result of the partitioning of tropical and extratropical warming activating relatively constant (across models) local feedbacks, then Eq. (10) should provide a reasonable approximation for model global effective feedbacks. On the other hand, if local feedback differences across models are important, then Eq. (9) may provide a more reasonable approximation of model global effective feedbacks. In the latter case, it is clear that local extratropical feedbacks are influenced by the magnitude of tropical warming (section 3); that is, ''local'' feedbacks are not strictly local. In both Eqs. (9) and (10), the pattern of warming is important, but by assessing these approximations, we will better understand the limits of the local feedback assumption.

Figure 9 shows the actual versus the approximated value of $\tilde{\lambda}_{\mathrm{lr}}$ for both assumptions. In computing the estimated global effective feedbacks from Eqs. (9) and (10), we use the zonal average values of the local feedbacks and surface warming pattern. Under the assumption that the local feedback strength is invariant across models [i.e., the meridional warming pattern activates local feedbacks that are held constant across models; see Eq. (10)], the estimated global effective feedback is correlated with the actual global effective feedback (Fig. 9a), but the range of the estimated feedbacks is much smaller than the actual feedbacks. When the global feedback is calculated under the assumption that the meridional pattern of surface warming is invariant across models [Eq. (9)], the estimated global feedback is much closer to the true values

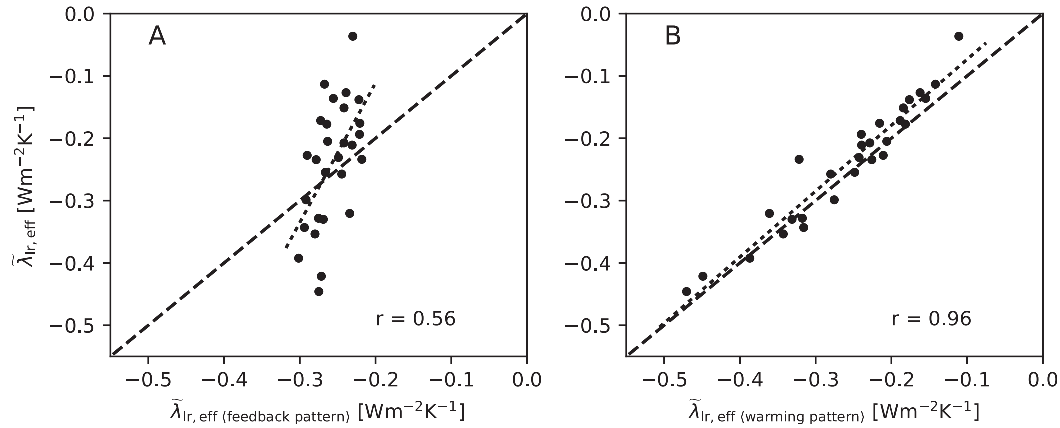

FIG. 9. The $\tilde{\lambda}_{\mathrm{lr,eff}}$ for each model vs the estimated feedback assuming that (a) local feedbacks are invariant [Eq. (10)] and (b) the meridional pattern of surface warming is invariant [Eq. (9)]. Note that in calculating the estimated feedbacks we used zonal mean local feedback fields and surface warming patterns (as in Fig. 3).

(Fig. 9b). These results show that differences in the strengths of the local feedbacks are an important factor in determining the magnitude of the global effective feedback. Although Fig. 9b shows results for $\tilde{\lambda}_{\mathrm{lr}}$ specifically, we note that we find similar results for the conventional LR and WV feedbacks.

Since the intermodel differences in the local feedback strength are important in estimating the global feedback, the model spread in the global effective feedback is not simply a result of model differences in polar amplification activating relatively constant local feedbacks, as was assumed in Armour et al. (2013). This does not imply, however, that the pattern of surface warming is unimportant. From section 3, it is clear that the strength of local feedbacks is a direct result of the meridional pattern of surface warming. The meridional pattern of surface warming modulates the global feedback both by controlling the ratio of polar and tropical local feedbacks and also by influencing the strength of subantarctic feedbacks.

The analysis thus far shows that model spread in local LR and WV feedbacks is an important contributor to intermodel variability in the global effective feedbacks. Given that most of the spread in the local feedbacks is concentrated in the subantarctic region, we should expect that this region is an important contributor to global feedback differences across models. We also know that the feedback in this region should be related to the partitioning of warming between the tropics and the extratropics [Eq. (7); Figs. 6c and 8d]. As a result, the global effective LR and WV feedbacks should be related to the equator-to-pole warming gradient in the Southern Hemisphere. In Fig. 10, we show the relationship between global $\tilde{\lambda}_{\mathrm{lr,eff}}$ and the ratio of tropical and extratropical surface warming for the Southern (Fig. 10a) and Northern Hemisphere (Fig. 10b). As expected, the relationship is stronger for the Southern Hemisphere, where intermodel variability in local feedbacks is much larger. Results are similar for the conventional global effective LR feedback. The conventional global effective WV feedback is also strongly related to the ratio of surface warming between the tropics and southern extratropics, but the relationship is weaker ($r = 0.74$) because some of the model spread in the water vapor feedback is due to relative humidity changes in the tropics (Figs. 3e and 7b). Although Arctic amplification of warming has been the focus of considerable scientific attention, our analysis points to the relative warming between the tropics and the Southern Hemisphere extratropics as an important contributor to intermodel differences in the LR and WV feedbacks.

The spread in local feedbacks is largest near 60°S at the margin between the Antarctic and subantarctic region (see Fig. 3) where changes in sea ice can interact with and amplify lapse rate and water vapor changes (Ramanathan 1977; Graversen et al. 2014; Feldl et al. 2017b). Furthermore, sea ice climatology may be important to simulated changes in the subantarctic region. Feldl et al. (2017b) studied the response of an ensemble of aquaplanet model simulations to a quadrupling of atmospheric CO_2. The albedo, LR, and WV feedbacks were strongly influenced by intermodel differences in the climatological albedo and sea ice extent values. After equilibrating to quadrupled CO_2 concentration, each model ended in the same ice-free state. A simple interpretation is that models with more climatological sea ice experience greater sea ice loss when subjected to a large external forcing. Zunz et al. (2013) show a similar result in simulations of historical climate change over 1979–2005 performed with CMIP5 atmosphere–ocean

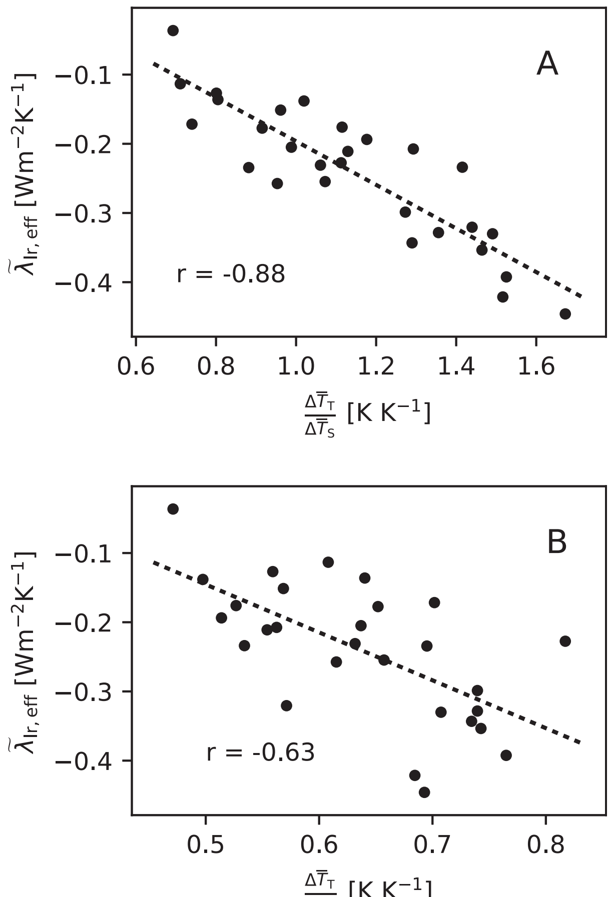

FIG. 10. (a) The $\tilde{\lambda}_{lr,eff}$ vs the ratio of tropical (30°N–30°S) and southern extratropical (30°–90°S) surface warming in each model. (b) The $\tilde{\lambda}_{lr,eff}$ vs the ratio of tropical and northern extratropical surface warming across GCMs.

GCMs, although the relationship between climatological sea ice extent and the change in sea ice extent exhibited substantial intermodel spread resulting from natural variability, the short time period considered, and the relatively modest forcing. Flato (2004) also found that climatological sea ice extent is significantly related to Antarctic surface temperature change in CMIP1 and CMIP2 simulations with CO_2 increases of 1% yr^{-1}. Like these studies, we also find that in simulations with large CO_2 forcing, model differences in Antarctic sea ice loss (Fig. 11a) and southern extratropical surface temperature change (Fig. 11b) are closely related to differences in sea ice climatology.

Recall that the global $\tilde{\lambda}_{lr,eff}$ is closely related to the ratio of tropical and southern extratropical surface warming (Fig. 10a). Since sea ice loss affects the magnitude of warming over the Southern Hemisphere, we expect that sea ice changes should be related to the global LR and WV feedbacks. This influence can be seen in Fig. 11c, which illustrates that there is a relationship between Antarctic sea ice loss and global $\tilde{\lambda}_{lr,eff}$ across models. Given that Antarctic sea ice loss is also tied to the model's initial sea ice extent, Antarctic sea ice climatology also plays a role in modulating the magnitude of $\tilde{\lambda}_{lr,eff}$ (Fig. 11d). Antarctic sea ice climatology also has a significant ($p < 0.05$) relationship with the global effective LR and WV feedbacks. This suggests that spread in the global effective LR and WV feedbacks is enhanced by intermodel differences in Antarctic sea ice climatology.

5. Summary

This analysis focuses on understanding intermodel differences in the LR and WV feedbacks. Past work has suggested that intermodel differences in global feedbacks can be better understood by introducing a framework that considers both spatially dependent local feedbacks and patterns of surface warming (Armour et al. 2013; Feldl and Roe 2013). For example, low-latitude warming produces vertical amplification of warming and a negative local LR feedback, whereas high-latitude warming is confined close to the surface, resulting in a positive local LR feedback. In turn, intermodel differences in polar amplification influence the relative contribution of these positive and negative feedbacks to the global average LR feedback. We show that although the balance of high- and low-latitude feedbacks is important, differences in the strength of local feedbacks across models, particularly in the SH, are the dominant component in explaining the intermodel spread in the global effective LR and WV feedbacks. Model-to-model differences in the strength of local feedbacks are closely related to model differences in the pattern of surface temperature change. In turn, the strength of the local feedbacks, and thus model global effective feedbacks, depends on the pattern of surface warming.

The Held and Shell (2012) definition of the local LR and WV feedbacks yields a useful geographic partitioning of local feedbacks. Using this framework, we show that model differences in relative humidity changes are largely confined to the tropics (Vial et al. 2013). As a result, $\tilde{\lambda}_{lr}$ is an excellent proxy for the sum of the LR and WV feedbacks in the extratropics, where both LR and WV feedbacks tend to have the largest intermodel spread. We therefore focused our analysis on the constant-RH LR feedback. Further research is necessary to understand the reasons for model differences in tropical relative humidity changes.

We shed light on model differences in local feedbacks by developing a linear framework to examine the LR

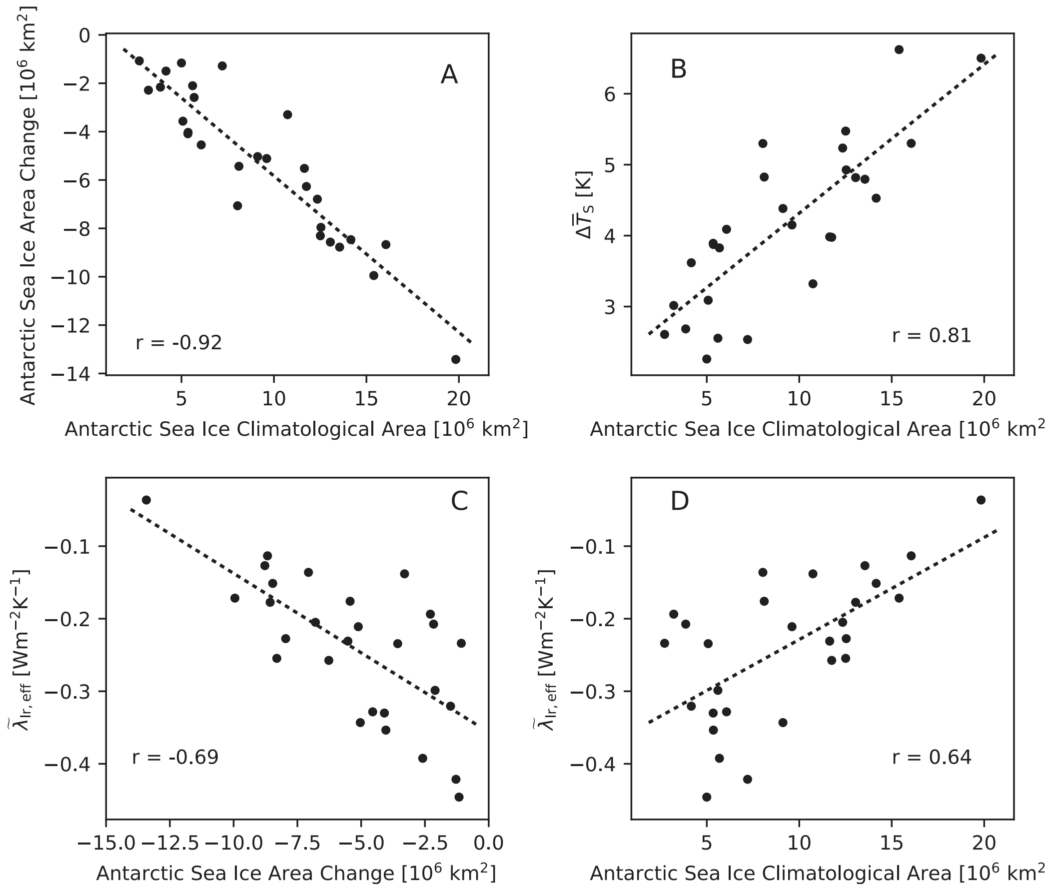

FIG. 11. (a) Change in the annual average Antarctic sea ice area vs the climatological annual average Antarctic sea ice area for each model. (b) Change in southern extratropical (30°–90°S) surface temperature vs the annual-mean climatological Antarctic sea ice area for each GCM. (c) The $\tilde{\lambda}_{\mathrm{lr,eff}}$ vs the change in the annual average Antarctic sea ice area for each model. (d) The $\tilde{\lambda}_{\mathrm{lr,eff}}$ vs the annual-mean Antarctic sea ice area climatology for each GCM.

and WV feedbacks in the tropics and extratropics. We show that the large-scale pattern of atmospheric warming and moistening is primarily a function of average surface warming over the tropics (30°S–30°N) and extratropics (30°–90°; see Butler et al. 2010; Screen et al. 2012; Po-Chedley 2016). In the tropics, where warming follows a moist adiabat, the tropical average LR feedback is approximately constant. Differences in model parameterizations for deep convection may help explain the relatively limited intermodel differences in the tropical LR feedback. The spread in the tropical WV feedback is also small; deviations across models are related to tropical RH changes. Intermodel differences in the tropical LR and WV feedbacks are not tied to a common physical mechanism and do not strongly covary. These results suggest that the well-documented correlation between the global LR and WV feedbacks across models does not arise from the covariation of the local tropical LR and WV feedbacks. Instead, the global LR and WV feedbacks are largely a function of the pattern of surface warming, which is a common control on both the extratropical LR and WV feedbacks.

Tropical surface warming induces an important nonlocal effect: it leads to a strong warming and moistening response in the tropical upper troposphere, which is then mixed poleward into the extratropics (Butler et al. 2010; Payne et al. 2015; Cronin and Jansen 2016; Rose and Rencurrel 2016). As a result, extratropical LR and WV feedbacks closely scale with the ratio between tropical and extratropical surface warming. This implies that tropical variability may dominate global climate feedback estimates derived from interannual variability (e.g., Dessler 2013), which could lead to estimates of $\tilde{\lambda}_{\mathrm{lr,eff}}$ that are too negative and not representative of long-term, equilibrated feedbacks. LR and WV feedbacks also contribute to changes in equilibrium climate sensitivity (ECS) over time, since $\tilde{\lambda}_{\mathrm{lr,eff}}$ becomes increasingly positive as subantarctic warming slowly

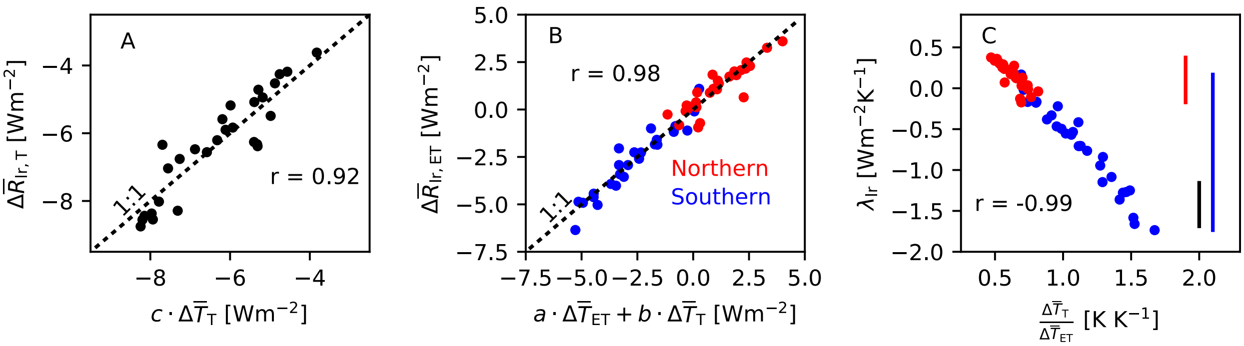

FIG. A1. As in Fig. 6, but for the LR feedback. Here, $a = 1.22$, $b = -1.71$, and $c = -1.40\,\mathrm{W\,m^{-2}\,K^{-1}}$.

emerges from the simulations considered here (e.g., Rose and Rayborn 2016). Because the extratropical LR and WV feedbacks are both controlled by the partitioning of tropical and extratropical surface warming, the extratropical LR and WV feedbacks are strongly correlated across models.

Model-to-model differences in the magnitude of local LR and WV feedbacks are three times larger in the Southern Hemisphere than in the Northern Hemisphere. Although the LR and WV feedbacks in both hemispheres are closely related to the ratio of tropical and extratropical surface warming $\overline{T}_T/\overline{T}_{\mathrm{ET}}$, the models consistently have amplified Northern Hemisphere surface warming and muted Southern Hemisphere surface warming relative to the tropics. The reduced southern extratropical surface warming results in an extratropical feedback that is particularly sensitive to the remote influence of the tropics. Further, surface warming in the northern extratropics is closely related to surface warming in the tropics across models ($r = 0.72$), which also reduces the spread in $\overline{T}_T/\overline{T}_{\mathrm{ET}}$.

We find that differences in local LR and WV feedbacks drive intermodel variability in the global effective feedbacks. Because model spread in the magnitude of local feedbacks is largest over the Southern Hemisphere, the local feedbacks over the Southern Hemisphere contribute strongly to the spread of the global effective LR and WV feedbacks. The relative warming between the tropics and southern extratropics determines the southern extratropical LR and WV feedbacks, and is therefore also an important influence on the global effective LR and WV feedbacks. Our analysis highlights the importance of the Southern Hemisphere in regulating the global LR and WV feedbacks in quasi-equilibrium climate simulations. Although it has long been known that the pattern of surface warming is important to understanding model differences in the global LR and WV feedbacks, we have shown here that these differences largely arise from differences in the magnitude of local extratropical feedbacks, particularly over the subantarctic region, which are controlled by the meridional pattern of surface warming.

Local feedbacks analyzed here do not solely respond to local surface temperature change. This implies that the traditional interpretation of local feedbacks, in which local feedbacks are constant in time, is not valid for the lapse rate and water vapor feedbacks. It is likely that other feedbacks (e.g., the cloud feedback) also respond to nonlocal processes (e.g., Mauritsen et al. 2013; Rose and Rayborn 2016; Zhou et al. 2016; Caldwell et al. 2016; Andrews and Webb 2018; Ceppi and Gregory 2017). While we show that local feedbacks are not time and model invariant, the local feedback framework can still be useful in interpreting global feedback differences across models, but with the understanding that a "local" feedback may not purely respond to local surface temperature.

As has been noted in other studies, we also find that intermodel differences in sea ice climatologies contribute to model differences in extratropical warming (e.g., Flato 2004; Feldl et al. 2017b). Since warming over the southern extratropics is an important component of the local and global LR and WV feedbacks, Antarctic sea ice climatology is significantly related to the global effective LR and WV feedbacks. Model differences in the representation of preindustrial Antarctic sea ice climatology contribute to the model spread in the global LR and WV feedbacks.

While several studies have used column or aquaplanet models to demonstrate the importance of nonlocal effects on lapse rate and water vapor changes (e.g., Payne et al. 2015; Cronin and Jansen 2016; Rose and Rencurrel 2016), our study shows that these nonlocal effects are also important in CMIP5 coupled atmosphere–ocean models. The nonlocal effect of tropical warming on the extratropical LR and WV feedbacks is greatest over the Southern Ocean, where upwelling mutes Southern Ocean warming (Armour et al. 2016) and leads to a clear

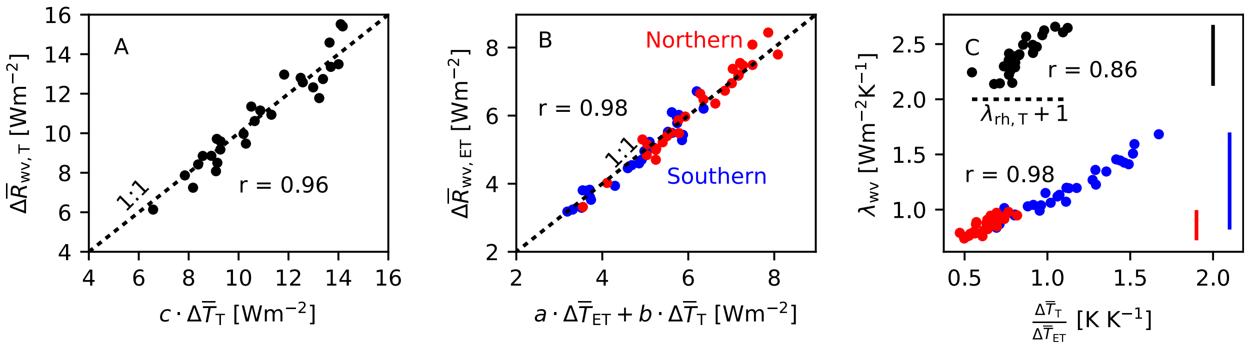

FIG. A2. As in Fig. 6, but for the WV feedback. Here, $a = 0.43$, $b = 0.68$, and $c = 2.41\ \mathrm{W\,m^{-2}\,K^{-1}}$. Note that the black dots in (c) represent the model tropical WV feedback plotted against the tropical RH feedback (plus one).

decoupling between surface warming and lapse rate and humidity changes (O'Gorman and Muller 2010; Rose and Rencurrel 2016). Although we have highlighted the LR and WV feedbacks over the Southern Ocean, zonal asymmetry in warming over the tropical Pacific Ocean is also likely to be enhancing the tropical LR and WV feedbacks over the observational record (Flannaghan et al. 2014; Ferraro et al. 2015; Zhou et al. 2016; Po-Chedley 2016). While it is clear that locally defined feedbacks can be influenced by nonlocal processes, we have shown that the local feedback framework is useful in understanding intermodel differences in global effective feedbacks.

Acknowledgments. S. P. was supported by the National Science Foundation (AGS-1624881) and the UW IGERT Program on Ocean Change (NSF Award 1068839). S. P. and Q. F. are also supported by the NASA Grant NNX13AN49G. C. M. B was supported by NSF PLR-1341497. The work of S. P., B. D. S., and M. D. Z. was performed under the auspices of the U.S. Department of Energy (DOE) by LLNL under Contract DE-AC52-07NA27344. Additional support was provided by the LLNL-LDRD Program under Project 18-ERD-054. M. D. Z. and B. D. S. are supported by the Regional and Global Climate Modeling Program of the DOE Office of Science. We acknowledge the World Climate Research Programme's Working Group on Coupled Modelling, which is responsible for CMIP, and we thank the climate modeling groups [see Caldwell et al. (2016) for a complete list] for producing and making available their model output. For CMIP, the U.S. Department of Energy's Program for Climate Model Diagnosis and Intercomparison provides coordinating support and led development of software infrastructure in partnership with the Global Organization for Earth System Science Portals. We thank Karl Taylor, Timothy Cronin, and two anonymous reviewers for providing helpful feedback on the manuscript.

APPENDIX

Analysis with Constant Relative Humidity Lapse Rate Feedback

Given the strong relationship between the lapse rate and water vapor feedbacks, our analysis largely focused on the constant-RH LR feedback. This feedback accounts for the radiative effects of lapse rate and water vapor changes at constant relative humidity (Fig. 2c). We note, however, that the scalings developed in Eqs. (4)–(8) also hold for the conventional lapse rate (Fig. A1) and water vapor (Fig. A2) feedbacks. While we have approximated the tropical feedbacks as constant, the tropical water vapor feedback does have some enhanced intermodel spread, which can be related to the relative humidity feedback. We demonstrate this in Fig. A2c.

REFERENCES

Andrews, T., and P. M. Forster, 2010: The transient response of global-mean precipitation to increasing carbon dioxide levels. *Environ. Res. Lett.*, **5**, 025212, https://doi.org/10.1088/1748-9326/5/2/025212.

——, and M. J. Webb, 2018: The dependence of global cloud and lapse rate feedbacks on the spatial structure of tropical Pacific warming. *J. Climate*, **31**, 641–654, https://doi.org/10.1175/JCLI-D-17-0087.1.

——, J. M. Gregory, and M. J. Webb, 2015: The dependence of radiative forcing and feedback on evolving patterns of surface temperature change in climate models. *J. Climate*, **28**, 1630–1648, https://doi.org/10.1175/JCLI-D-14-00545.1.

Armour, K. C., 2017: Energy budget constraints on climate sensitivity in light of inconstant climate feedbacks. *Nat. Climate Change*, **7**, 331–335, https://doi.org/10.1038/nclimate3278.

——, C. M. Bitz, and G. H. Roe, 2013: Time-varying climate sensitivity from regional feedbacks. *J. Climate*, **26**, 4518–4534, https://doi.org/10.1175/JCLI-D-12-00544.1.

——, J. Marshall, J. R. Scott, A. Donohoe, and E. R. Newsom, 2016: Southern Ocean warming delayed by circumpolar upwelling and equatorward transport. *Nat. Geosci.*, **9**, 549–554, https://doi.org/10.1038/ngeo2731.

Atwood, A. R., E. Wu, D. M. W. Frierson, D. S. Battisti, and J. P. Sachs, 2016: Quantifying climate forcings and feedbacks over the last millennium in the CMIP5–PMIP3 models. *J. Climate*, **29**, 1161–1178, https://doi.org/10.1175/JCLI-D-15-0063.1.

Bandoro, J., S. Solomon, A. Donohoe, D. W. J. Thompson, and B. D. Santer, 2014: Influences of the Antarctic ozone hole on Southern Hemispheric summer climate change. *J. Climate*, **27**, 6245–6264, https://doi.org/10.1175/JCLI-D-13-00698.1.

Bengtsson, L., S. Hagemann, and K. I. Hodges, 2004: Can climate trends be calculated from reanalysis data? *J. Geophys. Res.*, **109**, D11111, https://doi.org/10.1029/2004JD004536.

Bony, S., and Coauthors, 2006: How well do we understand and evaluate climate change feedback processes? *J. Climate*, **19**, 3445–3482, https://doi.org/10.1175/JCLI3819.1.

Butler, A. H., D. W. J. Thompson, and R. Heikes, 2010: The steady-state atmospheric circulation response to climate change–like thermal forcings in a simple general circulation model. *J. Climate*, **23**, 3474–3496, https://doi.org/10.1175/2010JCLI3228.1.

Caldwell, P. M., M. D. Zelinka, K. E. Taylor, and K. Marvel, 2016: Quantifying the sources of intermodel spread in equilibrium climate sensitivity. *J. Climate*, **29**, 513–524, https://doi.org/10.1175/JCLI-D-15-0352.1.

Ceppi, P., and J. M. Gregory, 2017: Relationship of tropospheric stability to climate sensitivity and Earth's observed radiation budget. *Proc. Natl. Acad. Sci. USA*, **114**, 13 126–13 131, https://doi.org/10.1073/pnas.1714308114.

Cess, R. D., 1975: Global climate change: An investigation of atmospheric feedback mechanisms. *Tellus*, **27** (3), 193–198, https://doi.org/10.3402/tellusa.v27i3.9901.

Colman, R. A., 2001: On the vertical extent of atmospheric feedbacks. *Climate Dyn.*, **17**, 391–405, https://doi.org/10.1007/s003820000111.

——, 2003: A comparison of climate feedbacks in general circulation models. *Climate Dyn.*, **20**, 865–873, https://doi.org/10.1007/s00382-003-0310-z.

Cronin, T. W., and M. F. Jansen, 2016: Analytic radiative-advective equilibrium as a model for high-latitude climate. *Geophys. Res. Lett.*, **43**, 449–457, https://doi.org/10.1002/2015GL067172.

Crook, J. A., P. M. Forster, and N. Stuber, 2011: Spatial patterns of modeled climate feedback and contributions to temperature response and polar amplification. *J. Climate*, **24**, 3575–3592, https://doi.org/10.1175/2011JCLI3863.1.

Dee, D. P., and Coauthors, 2011: The ERA-Interim reanalysis: Configuration and performance of the data assimilation system. *Quart. J. Roy. Meteor. Soc.*, **137**, 553–597, https://doi.org/10.1002/qj.828.

Deser, C., L. Sun, R. A. Tomas, and J. Screen, 2016: Does ocean coupling matter for the northern extratropical response to projected Arctic sea ice loss? *Geophys. Res. Lett.*, **43**, 2149–2157, https://doi.org/10.1002/2016GL067792.

Dessler, A. E., 2013: Observations of climate feedbacks over 2000–10 and comparisons to climate models. *J. Climate*, **26**, 333–342, https://doi.org/10.1175/JCLI-D-11-00640.1.

——, and S. M. Davis, 2010: Trends in tropospheric humidity from reanalysis systems. *J. Geophys. Res.*, **115**, D19127, https://doi.org/10.1029/2010JD014192.

Ding, Q., and Coauthors, 2017: Influence of high-latitude atmospheric circulation changes on summertime Arctic sea ice. *Nat. Climate Change*, **7**, 289–295, https://doi.org/10.1038/nclimate3241.

Dufresne, J.-L., and S. Bony, 2008: An assessment of the primary sources of spread of global warming estimates from coupled atmosphere–ocean models. *J. Climate*, **21**, 5135–5144, https://doi.org/10.1175/2008JCLI2239.1.

Elliott, W. P., and D. J. Gaffen, 1991: On the utility of radiosonde humidity archives for climate studies. *Bull. Amer. Meteor. Soc.*, **72**, 1507–1520, https://doi.org/10.1175/1520-0477(1991)072<1507:OTUORH>2.0.CO;2.

Feldl, N., and G. H. Roe, 2013: Four perspectives on climate feedbacks. *Geophys. Res. Lett.*, **40**, 4007–4011, https://doi.org/10.1002/grl.50711.

——, and S. Bordoni, 2016: Characterizing the Hadley circulation response through regional climate feedbacks. *J. Climate*, **29**, 613–622, https://doi.org/10.1175/JCLI-D-15-0424.1.

——, B. T. Anderson, and S. Bordoni, 2017a: Atmospheric eddies mediate lapse rate feedback and Arctic amplification. *J. Climate*, **30**, 9213–9224, https://doi.org/10.1175/JCLI-D-16-0706.1.

——, S. Bordoni, and T. M. Merlis, 2017b: Coupled high-latitude climate feedbacks and their impact on atmospheric heat transport. *J. Climate*, **30**, 189–201, https://doi.org/10.1175/JCLI-D-16-0324.1.

Ferraro, A. J., F. H. Lambert, M. Collins, and G. M. Miles, 2015: Physical mechanisms of tropical climate feedbacks investigated using temperature and moisture trends. *J. Climate*, **28**, 8968–8987, https://doi.org/10.1175/JCLI-D-15-0253.1.

Flannaghan, T. J., S. Fueglistaler, I. M. Held, S. Po-Chedley, B. Wyman, and M. Zhao, 2014: Tropical temperature trends in atmospheric general circulation model simulations and the impact of uncertainties in observed SSTs. *J. Geophys. Res. Atmos.*, **119**, 13 327–13 337, https://doi.org/10.1002/2014JD022365.

Flato, G. M., 2004: Sea-ice and its response to CO_2 forcing as simulated by global climate models. *Climate Dyn.*, **23**, 229–241, https://doi.org/10.1007/s00382-004-0436-7.

——, and Coauthors, 2013: Evaluation of climate models. *Climate Change 2013: The Physical Science Basis*, T. F. Stocker et al., Eds., Cambridge University Press, 741–866, https://www.ipcc.ch/pdf/assessment-report/ar5/wg1/WG1AR5_Chapter09_FINAL.pdf.

Frierson, D. M. W., 2006: Robust increases in midlatitude static stability in simulations of global warming. *Geophys. Res. Lett.*, **33**, L24816, https://doi.org/10.1029/2006GL027504.

——, 2008: Midlatitude static stability in simple and comprehensive general circulation models. *J. Atmos. Sci.*, **65**, 1049–1062, https://doi.org/10.1175/2007JAS2373.1.

Fu, Q., C. M. Johanson, S. G. Warren, and D. J. Seidel, 2004: Contribution of stratospheric cooling to satellite-inferred tropospheric temperature trends. *Nature*, **429**, 55–58, https://doi.org/10.1038/nature02524.

——, S. Manabe, and C. M. Johanson, 2011: On the warming in the tropical upper troposphere: Models versus observations. *Geophys. Res. Lett.*, **38**, L15704, https://doi.org/10.1029/2011GL048101.

Graversen, R. G., P. L. Langen, and T. Mauritsen, 2014: Polar amplification in CCSM4: Contributions from the lapse rate and surface albedo feedbacks. *J. Climate*, **27**, 4433–4450, https://doi.org/10.1175/JCLI-D-13-00551.1.

Gregory, J., and M. Webb, 2008: Tropospheric adjustment induces a cloud component in CO_2 forcing. *J. Climate*, **21**, 58–71, https://doi.org/10.1175/2007JCLI1834.1.

Hansen, J., A. Lacis, D. Rind, G. Russell, P. Stone, I. Fung, R. Ruedy, and J. Lerner, 1984: Climate sensitivity: Analysis of feedback mechanisms. *Climate Processes and Climate*

Sensitivity, *Geophys. Monogr.*, Vol. 29, Amer. Geophys. Union, 130–163.

Hartmann, D. L., and Coauthors, 2013: Observations: Atmosphere and surface. *Climate Change 2013: The Physical Science Basis*, T. F. Stocker et al., Eds., Cambridge University Press, 159–254, http://ipcc.ch/pdf/assessment-report/ar5/wg1/WG1AR5_Chapter02_FINAL.pdf.

Held, I. M., and B. J. Soden, 2000: Water vapor feedback and global warming. *Annu. Rev. Energy Environ.*, **25**, 441–475, https://doi.org/10.1146/annurev.energy.25.1.441.

——, and K. M. Shell, 2012: Using relative humidity as a state variable in climate feedback analysis. *J. Climate*, **25**, 2578–2582, https://doi.org/10.1175/JCLI-D-11-00721.1.

Holland, M. M., and C. M. Bitz, 2003: Polar amplification of climate change in coupled models. *Climate Dyn.*, **21**, 221–232, https://doi.org/10.1007/s00382-003-0332-6.

Laliberté, F., and P. J. Kushner, 2013: Isentropic constraints by midlatitude surface warming on the Arctic midtroposphere. *Geophys. Res. Lett.*, **40**, 606–611, https://doi.org/10.1029/2012GL054306.

Manabe, S., and R. T. Wetherald, 1975: The effects of doubling the CO_2 concentration on the climate of a general circulation model. *J. Atmos. Sci.*, **32**, 3–15, https://doi.org/10.1175/1520-0469(1975)032<0003:TEODTC>2.0.CO;2.

——, and R. J. Stouffer, 1980: Sensitivity of a global climate model to an increase of CO_2 concentration in the atmosphere. *J. Geophys. Res.*, **85**, 5529–5554, https://doi.org/10.1029/JC085iC10p05529.

——, ——, M. J. Spelman, and K. Bryan, 1991: Transient responses of a coupled ocean–atmosphere model to gradual changes of atmospheric CO_2. Part I. Annual mean response. *J. Climate*, **4**, 785–818, https://doi.org/10.1175/1520-0442(1991)004<0785:TROACO>2.0.CO;2.

Marshall, J., J. R. Scott, K. C. Armour, J.-M. Campin, M. Kelley, and A. Romanou, 2015: The ocean's role in the transient response of climate to abrupt greenhouse gas forcing. *Climate Dyn.*, **44**, 2287–2299, https://doi.org/10.1007/s00382-014-2308-0.

Mauritsen, T., R. G. Graversen, D. Klocke, P. L. Langen, B. Stevens, and L. Tomassini, 2013: Climate feedback efficiency and synergy. *Climate Dyn.*, **41**, 2539–2554, https://doi.org/10.1007/s00382-013-1808-7.

O'Gorman, P. A., and C. J. Muller, 2010: How closely do changes in surface and column water vapor follow Clausius–Clapeyron scaling in climate change simulations? *Environ. Res. Lett.*, **5**, 025207, https://doi.org/10.1088/1748-9326/5/2/025207.

Payne, A. E., M. F. Jansen, and T. W. Cronin, 2015: Conceptual model analysis of the influence of temperature feedbacks on polar amplification. *Geophys. Res. Lett.*, **42**, 9561–9570, https://doi.org/10.1002/2015GL065889.

Pithan, F., and T. Mauritsen, 2014: Arctic amplification dominated by temperature feedbacks in contemporary climate models. *Nat. Geosci.*, **7**, 181–184, https://doi.org/10.1038/ngeo2071.

Po-Chedley, S., 2016: On the structure of atmospheric warming in models and observations: Implications for the lapse rate feedback. Ph.D. thesis, University of Washington, 158 pp.

——, and Q. Fu, 2012: Discrepancies in tropical upper tropospheric warming between atmospheric circulation models and satellites. *Environ. Res. Lett.*, **7**, 044018, https://doi.org/10.1088/1748-9326/7/4/044018.

——, T. J. Thorsen, and Q. Fu, 2015: Removing diurnal cycle contamination in satellite-derived tropospheric temperatures: Understanding tropical tropospheric trend discrepancies. *J. Climate*, **28**, 2274–2290, https://doi.org/10.1175/JCLI-D-13-00767.1.

Proistosescu, C., and P. J. Huybers, 2017: Slow climate mode reconciles historical and model-based estimates of climate sensitivity. *Sci. Adv.*, **3**, e1602821, https://doi.org/10.1126/sciadv.1602821.

Ramanathan, V., 1977: Interactions between ice-albedo, lapse-rate and cloud-top feedbacks: An analysis of the nonlinear response of a GCM climate model. *J. Atmos. Sci.*, **34**, 1885–1897, https://doi.org/10.1175/1520-0469(1977)034<1885:IBIALR>2.0.CO;2.

Roe, G. H., N. Feldl, K. C. Armour, Y.-T. Hwang, and D. M. W. Frierson, 2015: The remote impacts of climate feedbacks on regional climate predictability. *Nat. Geosci.*, **8**, 135–139, https://doi.org/10.1038/ngeo2346.

Romps, D. M., 2014: An analytical model for tropical relative humidity. *J. Climate*, **27**, 7432–7449, https://doi.org/10.1175/JCLI-D-14-00255.1.

Rose, B. E. J., and L. Rayborn, 2016: The effects of ocean heat uptake on transient climate sensitivity. *Curr. Climate Change Rep.*, **2**, 190–201, https://doi.org/10.1007/s40641-016-0048-4.

——, and M. C. Rencurrel, 2016: The vertical structure of tropospheric water vapor: Comparing radiative and ocean-driven climate changes. *J. Climate*, **29**, 4251–4268, https://doi.org/10.1175/JCLI-D-15-0482.1.

——, K. C. Armour, D. S. Battisti, N. Feldl, and D. D. B. Koll, 2014: The dependence of transient climate sensitivity and radiative feedbacks on the spatial pattern of ocean heat uptake. *Geophys. Res. Lett.*, **41**, 1071–1078, https://doi.org/10.1002/2013GL058955.

Rugenstein, M. A. A., K. Caldeira, and R. Knutti, 2016: Dependence of global radiative feedbacks on evolving patterns of surface heat fluxes. *Geophys. Res. Lett.*, **43**, 9877–9885, https://doi.org/10.1002/2016GL070907.

Santer, B. D., and Coauthors, 2005: Amplification of surface temperature trends and variability in the tropical atmosphere. *Science*, **309**, 1551–1556, https://doi.org/10.1126/science.1114867.

——, and Coauthors, 2013: Human and natural influences on the changing thermal structure of the atmosphere. *Proc. Natl. Acad. Sci. USA*, **110**, 17 235–17 240, https://doi.org/10.1073/pnas.1305332110.

——, and Coauthors, 2014: Volcanic contribution to decadal changes in tropospheric temperature. *Nat. Geosci.*, **7**, 185–189, https://doi.org/10.1038/ngeo2098.

Schlesinger, M. E., and J. F. B. Mitchell, 1987: Climate model simulations of the equilibrium climatic response to increased carbon dioxide. *Rev. Geophys.*, **25**, 760–798, https://doi.org/10.1029/RG025i004p00760.

Screen, J. A., C. Deser, and I. Simmonds, 2012: Local and remote controls on observed Arctic warming. *Geophys. Res. Lett.*, **39**, L10709, https://doi.org/10.1029/2012GL051598.

Serreze, M. C., and J. A. Francis, 2006: The Arctic amplification debate. *Climatic Change*, **76**, 241–264, https://doi.org/10.1007/s10584-005-9017-y.

Sherwood, S. C., W. Ingram, Y. Tsushima, M. Satoh, M. Roberts, P. L. Vidale, and P. A. O'Gorman, 2010: Relative humidity changes in a warmer climate. *J. Geophys. Res.*, **115**, D09104, https://doi.org/10.1029/2009JD012585.

Singh, M. S., and P. A. O'Gorman, 2012: Upward shift of the atmospheric general circulation under global warming: Theory and simulations. *J. Climate*, **25**, 8259–8276, https://doi.org/10.1175/JCLI-D-11-00699.1.

Soden, B. J., and I. M. Held, 2006: An assessment of climate feedbacks in coupled ocean–atmosphere models. *J. Climate*, **19**, 3354–3360, https://doi.org/10.1175/JCLI3799.1.

——, ——, R. Colman, K. M. Shell, J. T. Kiehl, and C. A. Shields, 2008: Quantifying climate feedbacks using radiative kernels. *J. Climate*, **21**, 3504–3520, https://doi.org/10.1175/2007JCLI2110.1.

Stone, P. H., 1978: Baroclinic adjustment. *J. Atmos. Sci.*, **35**, 561–571, https://doi.org/10.1175/1520-0469(1978)035<0561:BA>2.0.CO;2.

Stouffer, R. J., and S. Manabe, 2017: Assessing temperature pattern projections made in 1989. *Nat. Climate Change*, **7**, 163–165, https://doi.org/10.1038/nclimate3224.

——, ——, and K. Bryan, 1989: Interhemispheric asymmetry in climate response to a gradual increase of atmospheric CO_2. *Nature*, **342**, 660–662, https://doi.org/10.1038/342660a0.

Taylor, K. E., R. J. Stouffer, and G. A. Meehl, 2012: An overview of CMIP5 and the experiment design. *Bull. Amer. Meteor. Soc.*, **93**, 485–498, https://doi.org/10.1175/BAMS-D-11-00094.1.

Thorne, P. W., 2008: Arctic tropospheric warming amplification? *Nature*, **455**, E1–E2, https://doi.org/10.1038/nature07256.

——, and R. S. Vose, 2010: Reanalyses suitable for characterizing long-term trends. *Bull. Amer. Meteor. Soc.*, **91**, 353–362, https://doi.org/10.1175/2009BAMS2858.1.

Vial, J., J.-L. Dufresne, and S. Bony, 2013: On the interpretation of inter-model spread in CMIP5 climate sensitivity estimates. *Climate Dyn.*, **41**, 3339–3362, https://doi.org/10.1007/s00382-013-1725-9.

Winton, M., K. Takahashi, and I. M. Held, 2010: Importance of ocean heat uptake efficacy to transient climate change. *J. Climate*, **23**, 2333–2344, https://doi.org/10.1175/2009JCLI3139.1.

Zelinka, M. D., and D. L. Hartmann, 2010: Why is longwave cloud feedback positive? *J. Geophys. Res.*, **115**, D16117, https://doi.org/10.1029/2010JD013817.

Zhou, C., M. D. Zelinka, and S. A. Klein, 2016: Impact of decadal cloud variations on the Earth's energy budget. *Nat. Geosci.*, **9**, 871–874, https://doi.org/10.1038/ngeo2828.

Zunz, V., H. Goosse, and F. Massonnet, 2013: How does internal variability influence the ability of CMIP5 models to reproduce the recent trend in Southern Ocean sea ice extent? *Cryosphere*, **7**, 451–468, https://doi.org/10.5194/tc-7-451-2013.